

SPID-Chain: A Smart Contract-Enabled, Polar-Coded Interoperable DAG Chain

AMIRHOSSEIN TAHERPOUR, Columbia University, USA

XIAODONG WANG, Columbia University, USA

As the digital landscape evolves, Web3 has gained prominence, highlighting the critical role of decentralized, interconnected, and verifiable digital ecosystems. This paper introduces SPID-Chain, a novel interoperability consensus designed for Web3, which employs a directed acyclic graph (DAG) of blockchains to facilitate seamless integration across multiple blockchains. Within SPID-Chain, each blockchain maintains its own consensus and processes transactions via an intra-consensus mechanism that incorporates event-driven smart contracts (EDSC) and Polar codes for optimized computation distribution. This mechanism is complemented by a division of committee and worker nodes, enhancing transaction processing efficiency within individual chains. For inter-blockchain consensus, SPID-Chain utilizes a DAG structure where blockchains append blocks containing cross-chain transactions. These blocks are then processed through the inter-consensus mechanism orchestrated by the blockchains. Extensive simulations validate the efficacy of our scheme in terms of throughput, scalability, decentralization, and security. Our results showcase SPID-Chain's potential to enable fluid interactions and transactions across diverse blockchain networks, aligning with the foundational goals of Web3.

Additional Key Words and Phrases: Web3, interoperability consensus, directed acyclic graph (DAG), smart contracts, Polar codes, Event-driven smart contracts (EDSC), scalability, security, decentralization.

1 INTRODUCTION

At present, the concept of Web3 is gaining momentum, heralding a new era of decentralized, interconnected, and verifiable digital ecosystems [1, 2]. Web3 envisions a fabric of interoperable blockchains, enabling seamless interactions and transactions across diverse networks. This vision extends beyond the mere exchange of data, encompassing the processing and validation of a myriad of transaction types in a distributed ledger ecosystem [3–5].

The evolution of blockchain technology has been marked by a shift from the initial focus on decentralization to a more nuanced emphasis on verifiability [6, 7]. While decentralization remains a cornerstone, the defining feature of Web3 has emerged as the ability to prove compliance with pre-agreed contractual terms within digital ecosystems, regardless of the underlying governance model or the complexity of the infrastructure [8, 9].

As we edge closer to this vision, the interoperability of blockchains becomes a crucial aspect of Web3, enabling a higher degree of efficiency and real-time responsiveness in various domains such as fintech [10], central banking [11], supply chain [12], and healthcare [13, 14]. For instance, consider a smart city framework where multiple blockchains orchestrate different facets of urban operations. Each blockchain, while optimizing operations within its domain, operates in isolation. However, a higher degree of efficiency and real-time responsiveness could be attained if these blockchains could communicate and reach consensus on cross-domain transactions [15, 16].

In the quest for blockchain interoperability, various approaches have emerged to address the challenges of connecting disparate blockchain networks. These approaches can be broadly categorized into five groups: *sidechains*, *notary schemes*, *hashed time lock contracts (HTLC)*, *relays*, and *blockchain-agnostic protocols* [17]. Each group offers unique mechanisms and protocols to facilitate the transfer of assets, data, and transactions between different blockchain systems. Next, we discuss the related works concerning these interoperability approaches in detail.

1.1 Related Works

To tackle the issue of blockchain interoperability, sidechains are employed. These are distinct blockchains linked to a primary blockchain, enabling asset exchanges in one or both directions. They enhance performance and facilitate asset utilization across different blockchain ecosystems. [18] proposes a sidechain method specifically for Proof-of-Stake (PoS) blockchains, introducing a cryptographic technique called ad-hoc threshold multi-signature (ATMS) for cross-chain certification, addressing security concerns such as the “goldfinger” attack in PoS blockchains. RootStock [19] is an example of a federated two-way peg sidechain for Bitcoin, which supports Ethereum-compatible smart contracts and uses a federation for asset management. Zendo [20] offers a flexible protocol using zk-SNARKs for secure communication between the mainchain and sidechains.

Notary schemes involve trusted entities, known as notaries, to validate transactions across blockchains. They can be centralized or decentralized, with the latter involving a group of notaries. [21] introduces a decentralized notary scheme for secure cryptocurrency trading, reducing dependence on a single trusted entity. ReviewChain [22] uses smart contracts and notaries for verifying cross-chain review data. Notary Group [23] presents a model using a group-based notary scheme for asset exchange, increasing reliability and reducing the risk of failure. RenVM [24] combines Byzantine fault-tolerant (BFT) consensus with secure multi-party computation (MPC) for trustless asset transfers. Bifrost [25] employs a notary scheme for sharing data across different blockchains.

HTLC enable trustless atomic swaps of cryptocurrencies, ensuring that transactions are either completed or rejected for all parties involved. TierNolan [26] is credited with the original atomic swap protocol based on HTLCs. Herlihy [27] extends this to support atomic swaps in complex scenarios involving multiple parties and blockchains. Burn-to-Claim [28] uses HTLCs for secure asset transfers between blockchains, involving burning assets on the source blockchain and recreating them on the destination blockchain.

Relays act as bridges for communication between different blockchain networks. BTCRelay [29] connects Bitcoin and Ethereum, allowing Ethereum users to verify Bitcoin transactions. XCLAIM [30] uses relays for trustless swaps between Bitcoin and Ethereum, employing a vault system for asset management. Verilay [31] is designed for Proof-of-Stake (PoS) blockchains, enabling validation of PoS protocols. Tesseract [32] uses Trusted Execution Environments (TEE) as trusted relays for secure cross-chain trades.

Blockchain-agnostic protocols provide a unified layer for interoperability across various blockchain networks. Interledger Protocol (ILP) v4 [33] supports secure and efficient asset transfers between different blockchains. Perun [34] enhances scalability by moving transactions off-chain into state channels. [35] propose a protocol for trusted data transfer across blockchain networks. Gravity [36] facilitates inter-blockchain communication and data exchange with an oracle consensus mechanism. Susy [36] builds on Gravity for cross-chain asset transfers, using oracle consensus for trust.

1.2 Motivation and Contributions

The above schemes have various drawbacks, which motivate us to propose our smart contract-enabled Polar-coded interoperable DAG chain (SPID-Chain). In particular, sidechains and notary schemes, while pioneering in enabling blockchain interoperability, grapple with significant scalability and security challenges. Sidechains, for instance, rely heavily on the underlying security of the primary blockchain and often struggle to manage increased load, leading to bottlenecks [38]. Notary schemes, whether centralized or decentralized, introduce external validators which can become potential points of failure and centralization, thus compromising the decentralized ethos of

blockchain technologies [39]. Our SPID-Chain’s introduction of a DAG ledger addresses these scalability concerns by allowing parallel processing of transactions, significantly enhancing throughput without compromising security. Moreover, our approach mitigates centralization risks associated with notary schemes by employing a bifurcated node architecture that ensures distributed validation without relying on a centralized group of validators [43].

HTLC and relay methods offer solutions for trustless asset swaps and communication between blockchains but often introduce high latency and operational complexity. These methods require locking assets into specific contracts with time-bound conditions, which can delay transaction completions and increase the complexity of multi-party transactions [40]. In contrast, our SPID-Chain utilizes an EDSC model that significantly reduces latency by responding to events rather than waiting for block confirmations. This model streamlines operations and enhances the user experience by facilitating quicker and more efficient interactions across blockchain networks [42].

Blockchain-agnostic protocols aim to create a unified layer for interoperability but often face challenges in maintaining efficiency and trust across diverse blockchain architectures. These protocols typically do not address the inherent differences in governance, consensus mechanisms, and transaction verification across chains, leading to inefficiencies and potential security vulnerabilities [41]. Our SPID-Chain’s use of Polar codes for the polarization of computations presents a novel approach to addressing these inefficiencies. By optimizing the distribution of computational tasks, SPID-Chain enhances fault tolerance and overall network efficiency, ensuring robust cross-chain interactions that are both secure and scalable [44, 45].

We summarize the deficiencies of the existing methods and our SPID-Chain’s solutions in Table.

1. The main contributions of this paper are as follows:

- (1) We introduce a novel interoperability consensus for Web3, leveraging a bifurcated node architecture and a unique combination of a DAG ledger for inter-consensus and smart contracts for intra-consensus. This approach optimizes governance, validation processes, and computational workload distribution, enhancing both security and performance in a decentralized digital realm.
- (2) Our SPID-Chain features several innovative mechanisms, including the polarization of computations using Polar codes to address the straggler problem and improve fault tolerance, and an event-driven smart contract (EDSC) model that surpasses traditional transaction-driven models in scalability, latency, and security.
- (3) Through extensive simulations, our comprehensive scheme for cryptocurrency Web3 networks demonstrates excellent performances in terms of throughput, scalability, decentralization, security, and latency, showcasing its potential to facilitate seamless interactions and transactions across disparate blockchain networks.

The remainder of the paper is organized as follows: Section 2 outlines the SPID-Chain architecture, discussing the consensus mechanisms and detailing cross-chain interactions via the DAG ledger. Section 3 examines the intra-consensus mechanism in SPID-Chain, focusing on event-driven smart contracts and their interactions with various network components. Section 4 presents the application of SPID-Chain in cryptocurrency Web3 networks. In Section 5, we provide simulation results to evaluate the scheme’s performance on metrics such as throughput, scalability, decentralization, and security. Section 6 provides the conclusion of the paper.

2 SPID-CHAIN

In this section, we first provide an overview of our proposed SPID-Chain and its consensus mechanisms. Then we describe cross-chain interactions through the DAG ledger.

Table 1. Challenges and SPID-Chain Solutions for Blockchain Interoperability

Interoperability Approach	Challenges	SPID-Chain Solutions
Sidechains	<ul style="list-style-type: none"> • Scalability bottlenecks due to dependency on the main chain's security • Security dependency on the main chain 	<ul style="list-style-type: none"> • DAG ledger allows parallel processing, improving scalability and throughput • Independent security with bifurcated node architecture
Notary Schemes	<ul style="list-style-type: none"> • Centralization risks • Potential single points of failure 	<ul style="list-style-type: none"> • Distributed validation reduces centralization and enhances security • Improves fault tolerance with innovative node architecture
HTLC and Relays	<ul style="list-style-type: none"> • High latency • Operational complexity in multi-party transactions 	<ul style="list-style-type: none"> • Event-driven smart contracts reduce latency by processing transactions based on events • Simplifies cross-chain interactions, reducing dependency on sequential confirmations
Blockchain-Agnostic Protocols	<ul style="list-style-type: none"> • Efficiency issues across diverse networks • Trust and verification concerns 	<ul style="list-style-type: none"> • Utilizes Polar codes for efficient computational task distribution • Enhances fault tolerance and security with distributed coded computing

2.1 System Overview

We consider a Web3 network consisting of N interconnected blockchains. We categorize nodes in each blockchain into two groups: committee nodes and worker nodes. Committee nodes are key players in the governance and validation processes within the chain, responsible for overseeing transactions and ensuring the integrity of the blockchain's operations. Worker nodes, on the other hand, are tasked with executing computational work regarding processing the transactions. This bifurcation of roles allows for a more efficient and organized approach to managing blockchain operations, ensuring both security and performance.

SPID-Chain's consensus mechanism comprises two key components: intra-consensus and inter-consensus. The intra-consensus component facilitates interactions among nodes within each blockchain, whereas the inter-consensus component is essential for achieving consensus across the blockchains, particularly for processing cross-chain transactions. Consequently, all interactions related to the intra-consensus of each chain are stored on its respective ledger. In contrast, data pertaining to cross-chain transactions and interactions among the blockchains are recorded on a

DAG ledger. Therefore, while each blockchain maintains its individual ledger, the DAG ledger is collectively stored and managed by all blockchains.

Hence, within each chain committee nodes are cherry-picked from the ensemble of full nodes. Each full node possesses a complete copy of the blockchain’s ledger. Specifically, the ledger for each chain j maintained by full nodes is composed of two distinct parts. The first part includes data specific to chain j , such as events related to the activation of smart contracts or information pertinent to committee selection (detailed in Section 3). The second part comprises data common to all N chains, which includes the information contained in the blocks existing on the DAG. On the other hand, worker nodes, categorized as light nodes, retain only a fraction of the chain’s ledger in a coded format. Note that light nodes overwrite old data with new data, thereby sustaining a constant data storage requirement.

Table 2. Consensus mechanisms in SPID-Chain.

Consensus Type	Consensus Level	Mechanism/Tool	Purpose/Function
Inter-Consensus	Blockchain-Blockchain	DAG Ledger	Facilitates harmonious cross-chain transaction processing and data sharing across diverse blockchains, enhancing network interoperability.
Intra-Consensus	Committee-Committee Member	Smart Contracts	Oversees the decision-making process within committee nodes, crucial for the trustworthy creation of new blocks.
	Committee-Worker Member	Coded Distributed Computing	Enables efficient task execution and workload distribution, strengthening the cooperation between committee and worker nodes.

Our SPID-Chain, employs distinct mechanisms for managing both intra-consensus and inter-consensus processes, as outlined in Table 2. The DAG ledger is adeptly chosen for the blockchain-blockchain consensus due to its ability to handle a high volume of transactions efficiently. In contrast to traditional blockchains, where a linear sequence of blocks can slow down processing time, the DAG structure allows each node to add transactions independently without the need for synchronization across the entire network. This decentralized approach significantly enhances the scalability and speed of transaction processing. Moreover, the DAG ledger’s architecture is particularly suited for Web3 environments where multiple blockchains operate concurrently and asynchronously. By allowing each blockchain to contribute independently while maintaining a coherent global state, the DAG ledger ensures a smooth and efficient interoperability, which is critical for the robustness and reliability of a Web3 ecosystem.

Also, in the proposed interoperability consensus, smart contracts serve as a crucial component enhancing both automation and security. Their primary function is to automate the decision-making processes, ensuring a fair and secure method for orchestration of the tasks in the network. Additionally, the integration of event logging within smart contracts is a significant advancement. This feature allows for the verification of function execution through logs, rather than requiring other committee nodes to re-execute the function. This approach is efficient in terms of resource utilization and time management. It also enhances security by providing a consistent and verifiable record of executions, thereby reducing the risk of discrepancies.

Moreover, coded distributed computing is strategically employed in the committee-worker member consensus to manage and optimize computational tasks. This is particularly vital in handling large-scale data inherent to Web3 environments. Coded distributed computing not only aids in mitigating the impact of stragglers and enhancing fault tolerance but also plays a pivotal role in reaching consensus. The latter is achieved by treating the computations performed by worker nodes as a form of “voting” for consensus. The final consensus value of the network is derived from these computational results, thereby ensuring that consensus is reached not only efficiently but also with the inherent benefits of fault tolerance and straggler mitigation.

2.2 SPID-Chain Inter-consensus

In this subsection we first address inter-consensus interaction detailing how blockchains contribute to the DAG ledger in defined epochs. This is followed by discussing the consensus used for blocks on the DAG.

2.2.1 Inter-Consensus Interaction. Time is divided into epochs, and in each epoch t , every blockchain j has a primary objective: to generate and contribute a block, referred to as $Z_j^P(t)$, to the DAG ledger. This *proposed* block comprises transactions initiated within blockchain j and represents its contribution to that epoch. $Z_j^P(t)$ then undergoes a consensus process (details in Section 2.2.2) after being appended to the DAG ledger. If successful, it transitions from a proposed to a *confirmed* state, denoted as $Z_j^C(t)$, thereby finalizing the transactions it contains.

In each epoch t , blockchain j follows a specific process to generate its proposed block $Z_j^P(t)$. Initially, it compiles all incoming transactions into a block, denoted as $X_j^P(t)$. To validate these transactions and formulate the proposed block, it references its cumulative history of confirmed blocks, denoted as $\mathcal{Y}_j(t)$, comprising all confirmed super-blocks $Y_j^C(t')$ added to blockchain j 's ledger from the genesis block up to the conclusion of the previous epoch $t - 1$, i.e., $1 \leq t' \leq t - 1$. Each of these super-blocks $Y_j^C(t')$ contains a set of confirmed blocks $Z_i^C(t'')$ on the DAG, i.e., the proposed block of chain i in epoch t'' that is confirmed in epoch $t' - 1$. To create the corresponding block $Y_j^C(t')$ for each epoch t' , chain j selects one confirmed block from each of the N chains, provided that each chain has at least one confirmed block during epoch t' . If a chain has more than one confirmed block, chain j randomly chooses one of these blocks to include in $Y_j^C(t')$. If a chain does not have any confirmed blocks, it is not included in $Y_j^C(t')$. Thus by using $\mathcal{Y}_j(t)$ as a reference for validation, chain j ensures that the transactions in the proposed block $Z_j^P(t)$ are legitimate and align with the most recent blockchain history. Chain j then integrates the validated transactions in $X_j^P(t)$ into $Z_j^P(t)$ and submits it to the DAG ledger as its contribution to that epoch.

2.2.2 DAG Ledger in Detail. By using a modified IOTA Coordicide [47] consensus mechanism as described next, our SPID-Chain employs a DAG ledger to facilitate cross-chain interactions and enhance interoperability in consensus mechanisms.

To submit the contributed block $Z_j^P(t)$ for epoch t to the DAG, chain j generates a super-block $Z_j^T(t)$ comprising K randomly selected tip blocks for validation, resulting in $Z_j^V(t)$ the subset of valid blocks in $Z_j^T(t)$ using the information in the ledger $\mathcal{Y}_j(t) = \bigcup_{t'=1}^{t-1} Y_j^C(t')$. It then integrates $Z_j^P(t)$ into the DAG by selecting the blocks in $Z_j^V(t)$ as its predecessors, thereby establishing directed edges from the vertex of $Z_j^P(t)$ to each block in $Z_j^V(t)$. As a result of above actions performed by all chains, the aggregated weight (AW) of the blocks on the DAG changes. This leads to a change in the validity status of some blocks on the DAG. Specifically, certain proposed blocks, such as $Z_i^P(t')$, are confirmed, and their status are updated to $Z_i^C(t')$. Next, we explain how the AW of each block on the DAG is altered and how the transition from a proposed to a confirmed status occurs.

Fig. 1 illustrates a DAG ledger for two consecutive epochs $t - 1$ and t . In epoch $t - 1$, each vertex represents a proposed block $Z_{j_i}^P(t_i)$ by blockchain j_i , for $i = 1, \dots, 4$, at epoch $t_i < t - 1$. A direct edge from one vertex to another, for example, from $Z_{j_2}^P(t_2)$ to $Z_{j_1}^P(t_1)$, signifies that j_2 verifies block $Z_{j_1}^P(t_1)$. Fig. 1 also displays the status evolution of the blocks after one epoch. A block is labeled as a *tip* if it lacks incoming validation edges. Therefore, in this figure, for epochs $t - 1$ and t , the blocks $\{Z_{j_2}^P(t_2), Z_{j_3}^P(t_3), Z_{j_4}^P(t_4)\}$ and $\{Z_{j_5}^P(t_5), Z_{j_6}^P(t_6)\}$ are tip blocks, respectively.

Moreover, a block that is neither a tip nor confirmed is referred to as an unconfirmed block. Hence, while blocks $\{Z_{j_2}^P(t_2), Z_{j_3}^P(t_3), Z_{j_4}^P(t_4)\}$ are tips in epoch $t - 1$, block $Z_{j_3}^P(t_3)$ is classified as unconfirmed in epoch t , while $\{Z_{j_2}^P(t_2), Z_{j_4}^P(t_4)\}$ remain as tips. Observe that the status of $Z_{j_1}^P(t_1)$, transitions from proposed to confirmed, which is denoted by $Z_{j_1}^C(t_1)$. Specifically, a block achieves confirmed status when its AW surpasses a predefined threshold η . The AW is intricately linked to a weight vector that reflects the relative influence of the N blockchains.

The weight ω_j of each blockchain j with $\omega_j > 0$, $\sum_{j=1}^N \omega_j = 1$ is determined by the number of tokens it has staked, and this weight is assumed to remain constant over different epochs. However, if blockchain j acts maliciously, ω_j will be adjusted accordingly, as some of the staked tokens will be burnt. Essentially, the greater the number of tokens a blockchain stakes, the more significance the network assigns to its validations.

The AW of a block $Z_{j_i}^P(t_i)$ is calculated as $\omega_i + \sum_{Z_{j_{i'}}^P(t_{i'}) \in \mathcal{F}(Z_{j_i}^P(t_i))} \omega_{j_{i'}}$, where $\mathcal{F}(Z_{j_i}^P(t_i))$ denotes the future cone of $Z_{j_i}^P(t_i)$, encompassing all blocks that it validates, either directly or through a series of validations. For example, in Fig. 1 and in epoch t , blocks $\{Z_{j_1}^P(t_1), Z_{j_4}^P(t_4)\}$ are in the future cone of block $Z_{j_6}^P(t_6)$, as block $Z_{j_4}^P(t_4)$ is validated by it directly, while block $Z_{j_6}^P(t_6)$ validates block $Z_{j_1}^P(t_1)$ indirectly. Therefore, Fig. 1 illustrates the AW for the corresponding DAG ledgers, indicating, for example, how the AW of block $Z_{j_1}^P(t_1)$ surpasses η and its status evolves from an unconfirmed block to confirmed after the addition of the weights of blocks $Z_{j_5}^P(t_5)$ and $Z_{j_6}^P(t_6)$ since block $Z_{j_1}^P(t_1)$ is in the future cone of blocks $Z_{j_5}^P(t_5)$ and $Z_{j_6}^P(t_6)$.

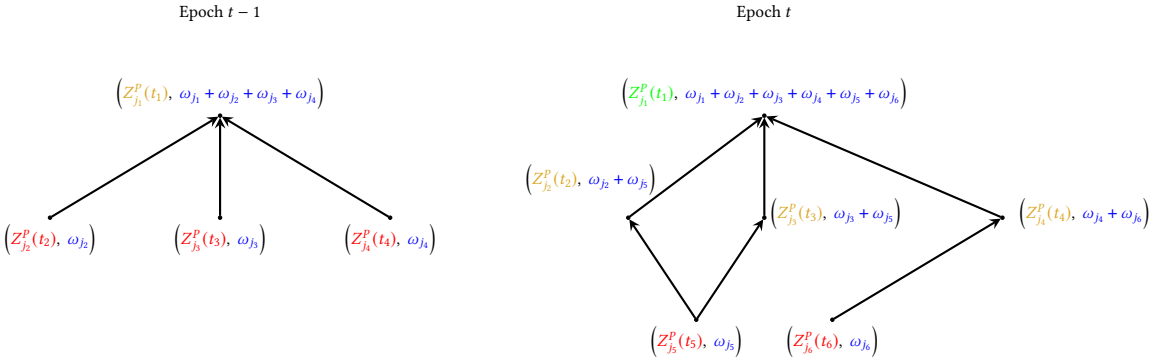


Fig. 1. Evolution of a DAG ledger over two consecutive epochs. Nodes are color-coded to indicate their status: yellow for unconfirmed, green for confirmed, and red for tips. The blue text represents the AW associated with each node.

3 INTRA-CONSENSUS IN SPID-CHAIN

In this section, we present the intra-consensus mechanism in SPID-Chain, focusing on the utilization of Event-Driven Smart Contracts (EDSC) and their interaction with oracles, committee nodes, and

worker nodes. We discuss the role of smart contracts in various stages of consensus and outline the process for committee member selection and event validation to ensure network integrity and security.

3.1 EDSC in SPID-Chain

3.1.1 Background on EDSC. Our SPID-Chain makes use of EDSC, which diverges from conventional smart contracts by leveraging three pivotal concepts: event definition, event subscription, and event publishing. These elements collectively enable a dynamic and responsive blockchain network.

Event definition involves delineating the characteristics of an event within the blockchain, such as changes in data values or the execution of specific actions. Once defined, these events are immutably recorded, ensuring security and permanence. Event subscription then follows, where smart contracts express interest in specific events. This phase involves integrating additional logic within the subscribing contracts, allowing for a tailored response when the event occurs. The process culminates with event publishing, where the occurrence of an event is broadcast across the blockchain. This update triggers the subscribed smart contracts to autonomously execute predefined actions, based on their subscription logic.

These three stages form the backbone of the EDSC framework, enhancing the functionality and specificity of smart contracts within the blockchain ecosystem. The adoption of EDSC brings forth several advantages [46]. Firstly, it addresses scalability challenges by utilizing an event-driven model, allowing for more efficient processing and reduced network strain. This leads to improved performance and scalability. Secondly, the asynchronous nature of event handling in EDSC contributes to reduced latency in smart contract execution, enhancing system responsiveness. Additionally, EDSC's architecture inherently offers enhanced security features, mitigating the risk of certain attacks and ensuring that the execution of one contract does not directly impact others. Finally, the framework is well-suited for integrating external data through oracles, enabling more dynamic and responsive smart contract applications. Overall, EDSC represents a significant advancement in the realm of smart contracts, offering a more scalable, secure, and efficient framework for the blockchain ecosystem.

3.1.2 Oracle, Committee Nodes, and Worker Nodes. As we discussed, during each epoch t , the goal of each blockchain j is to contribute a block $Z_j^P(t)$ through an intra-consensus mechanism. This mechanism relies on EDSC, which orchestrates consensus stages using a set of six blocks $\{C_j^k\}_{k=1}^6$ each containing a smart contract for specific intra-consensus tasks, and an oracle that publishes events to trigger these smart contracts. Moreover, in each epoch t , nodes in each blockchain j are split into committee members ($C_j(t)$) and workers ($W_j(t)$) for intra-consensus.

The oracle acts as a bridge between external data sources and the blockchain, generating events based on information provided by committee nodes or results from worker nodes. These events are then published to the network, where they await validation.

Committee nodes, responsible for maintaining the integrity and security of the network, validate the events published by the oracle. They ensure that the events meet predefined criteria and are legitimate triggers for the smart contracts. Additionally, the highest-ranked committee node has the crucial role of feeding the oracle with information necessary for event generation, including transaction details, network conditions, or other relevant data.

Worker nodes come into play when a smart contract for processing is activated by a validated event. They are responsible for executing assigned tasks, such as processing data or performing computations. Upon completing their tasks, worker nodes submit the results to the oracle, potentially leading to the generation of new events.

3.2 Smart Contracts and Consensus on Events

3.2.1 Smart Contracts in SPID-Chain. In our proposed scheme, each blockchain operates based on a sequence of stages in each epoch, with smart contracts playing a crucial role in ensuring compliance with these stages. We define smart contracts in six blocks, denoted as $\{C_j^k\}_{k=1}^6$, each designed to listen for specific events and activate at the appropriate times.

The events that trigger these smart contracts are predefined and can be published by various occurrences within the network. These occurrences include, but are not limited to, changes in data values and the execution of specific actions. The events are generated based on information provided by the network's nodes and are crucial for the realization of different stages within each epoch.

The first smart contract, C_j^1 , is subscribed to the event published by the oracle pertaining to the formation of the transaction block $X_j^P(t)$ initiated by accounts in chain j through committee nodes. This contract delegates the necessary computations to worker nodes for processing block $X_j^P(t)$. Consequently, the objective of this block is to assist committee nodes in first reaching consensus on $X_j^P(t)$, and second, on delineating the set of tasks to be assigned to worker nodes for processing $X_j^P(t)$.

The second smart contract, C_j^2 , is subscribed to the event published by the oracle, which includes the computation results from worker nodes assigned by C_j^1 . It generates $Z_j^P(t)$, the proposed block in epoch t by chain j , contingent on the committee nodes' consensus on the validity of the published event. Thus, this contract aids in the consensus between worker and committee nodes for the creation of $Z_j^P(t)$. The computation results from the workers effectively act as votes on the validity of transactions in $X_j^P(t)$, leading to the selection of valid transactions and the generation of $Z_j^P(t)$. Additionally, as discussed later in Section 3.2.2, the event that triggers C_j^2 is verified by committee nodes and only activates C_j^2 if there is consensus on its validity, further underscoring this contract's role in facilitating committee-worker consensus.

The third smart contract, C_j^3 , is subscribed to the event published by the oracle regarding the formation of the super-block $Z_j^T(t)$ for processing the tip blocks on the DAG by committee nodes. Analogous to C_j^1 , the purpose of C_j^3 is to aid committee nodes in reaching consensus on both $Z_j^T(t)$ and the set of tasks to be assigned to worker nodes for processing $Z_j^T(t)$.

The fourth smart contract, C_j^4 , is subscribed to the event published by the oracle concerning the reception of computation results from worker nodes assigned by C_j^3 . The goal of this contract is to identify the super-block $Z_j^V(t)$, which consists of valid blocks in $Z_j^T(t)$. Similar to C_j^2 , the purpose of C_j^4 is to facilitate consensus between worker and committee nodes for the creation of super-block $Z_j^V(t)$.

The fifth smart contract, C_j^5 , is subscribed to the event published by the oracle regarding the discovery and formation of $Z_j^V(t)$ by committee nodes. The role of this contract is to submit the proposed block $Z_j^P(t)$ to the DAG, update the AW of current blocks on the DAG, and, if eligible, change their status to confirmed. Hence, C_j^5 assists committee nodes in reaching consensus on the *compliance* of submitting block $Z_j^P(t)$ to the DAG as per the prescribed protocol.

The sixth and final smart contract, C_j^6 , is subscribed to the event published by the oracle concerning the formation of the super-block $Y_j^C(t)$, which consists of confirmed blocks on the DAG by the committee nodes. The purpose of this contract is to update the ledger $\mathcal{Y}_j(t)$. Similar to C_j^5 , this

contract aids committee nodes in reaching consensus on the accuracy of $Y_j^C(t)$, the super-block added to the ledger in epoch t .

In summary, the smart contracts C_j^1 , C_j^3 , C_j^5 , and C_j^6 primarily facilitate consensus among committee nodes, while C_j^2 and C_j^4 aim to enable consensus between committee and worker nodes.

3.2.2 Committee Member Selection and Event Validation. The selection of committee members is based on a probability proportional to their stakes or reputations. Specifically, each node within a blockchain engenders a Verifiable Random Function (VRF) output utilizing their private key and a shared random seed, contingent on the current epoch time t . The VRF outputs are then used to determine the selection probability, with nodes boasting larger stakes or elevated reputations standing a higher chance of being elected as committee members. This mechanism not only earmarks the committee members but also ensures a fair and secure selection process vital for the network's integrity.

For smart contracts C_j^1 , C_j^3 , C_j^5 , and C_j^6 , committee nodes follow the following protocol to validate the published events by the oracle and handle the interactions with those smart contracts. The highest-ranked committee node feeds the relevant information to the oracle. The oracle publishes an event corresponding to the fed information. The published event acts as a proposed event, which is then validated by other committee members. This validation involves ensuring that the event proposal adheres to the agreed-upon criteria and rules, similar to how transaction validation works. The proposed event is subject to a vote by the committee members. If the majority approves the event, it becomes an active event. Now this active event triggers the corresponding smart contract that is subscribed to it. If the proposed event does not receive majority approval, it is discarded, and the next highest-ranked node gets the opportunity to propose an event by submitting the information to the oracle, leading the publication of a proposed event which in case of consensus on its validity will be an active event that will trigger the smart contract subscribed to it. This process continues until an event proposal gains the required majority consensus and executes its predefined logic based on the event data.

The protocol for activating the smart contracts C_j^2 and C_j^4 shares a similar structure with that of C_j^1 , C_j^3 , C_j^5 , and C_j^6 , with a focus on facilitating consensus between committee and worker nodes. In this process, the oracle publishes a proposed event containing computation results from worker nodes. Committee nodes validate this event, and if it receives majority approval, it triggers the corresponding smart contract.

The approach of utilizing decentralized control in the execution of smart contracts offers several advantages. Firstly, it ensures that no single node possesses unilateral control over the triggering of smart contracts. This is because the activation of these contracts is subject to the approval of a committee, preventing any one entity from having excessive power. Additionally, this method significantly enhances security and integrity. The rank-based consensus required for event triggers means that only events that have been thoroughly vetted and approved can activate the smart contracts, thereby ensuring a higher level of trustworthiness and reliability in their execution. Furthermore, this approach retains the flexibility and efficiency inherent in EDSC. Smart contracts continue to be triggered by events, yet they benefit from an added layer of security through the decentralized consensus mechanism. This combination of decentralized control, enhanced security, and maintained efficiency makes this approach particularly effective in the management and execution of smart contracts in SPID-Chain.

4 SPID-CHAIN FOR CRYPTOCURRENCY WEB3 NETWORKS

4.1 Balance Checking

We consider a fundamental Web3 cryptocurrency framework designed to monitor balance transfers between accounts. We assume that each blockchain is linked to M accounts or addresses. The matrix $\mathbf{X}_{\ell,\ell'}(t) \in \mathbb{R}^{M \times M}$ aggregates M transactions within epoch t . Specifically, a transaction within this block that involves account m on chain ℓ transferring s tokens to account m' on chain ℓ' is expressed as $\mathbf{X}_{\ell,\ell'}(t)[m, m'] = s$. Accounts that do not participate in sending tokens have their corresponding matrix entries set to zero.

To verify blocks for each chain j in each epoch t , represented as $X_j^P(t) = \{\mathbf{X}_{j,\ell}(t)\}_{\ell=1}^N$, we denote by $P_j^t(X_j^P(t), \mathcal{Y}_j(t)) = Z_j^P(t)$ the operation that takes the formed block $X_j^P(t)$ in epoch t and the data $\mathcal{Y}_j(t)$ in the ledger updated up to epoch t and returns the proposed block $Z_j^P(t) = \{\mathbf{Z}_{j,\ell}(t)\}_{\ell=1}^N$ of chain j for epoch t to attach to the DAG. To do so, for blocks $\{\mathbf{X}_{j,\ell}(t)\}_{\ell=1}^N$ it is essential to confirm that all sending accounts possess sufficient unspent funds from preceding transactions. Let $\{\mathbf{Y}_{j,\ell}(r)\}_{\ell=1}^N$ represent the blocks confirmed from ledger $\mathcal{Y}_j(t)$ that detail transactions spending tokens from accounts on chain j in epoch r . Similarly, $\{\mathbf{Y}_{\ell,j}(r)\}_{\ell=1}^N$ refers to the blocks containing transactions that deposit tokens into accounts on chain j over the same epoch. We further define

$$\begin{aligned} \mathbf{A}_j(r) &= \sum_{\ell=1, \ell \neq j}^N \mathbf{Y}_{\ell,j}(r), \\ \mathbf{B}_j(r) &= \sum_{\ell=1, \ell \neq j}^N \mathbf{Y}_{j,\ell}(r), \quad r = 1, \dots, t, \\ \mathbf{C}_j(t) &= \sum_{\ell=1, \ell \neq j}^N \mathbf{X}_{j,\ell}(t). \end{aligned} \tag{1}$$

Here $\mathbf{A}_j(r)$ captures the total tokens received by chain j from all other chains in epoch r ; $\mathbf{B}_j(r)$ accounts for the total tokens dispatched from chain j to all other chains during the same epoch, and $\mathbf{C}_j(t)$ denotes the tokens spent by chain j across all other chains in a given epoch t .

Remark 1: It is important to distinguish between $\mathbf{X}_{j,\ell}(t)$, $\mathbf{Z}_{j,\ell}(t)$, and $\mathbf{Y}_{j,\ell}(t)$ in terms of their roles within the transaction validation process. The block $\mathbf{X}_{j,\ell}(t)$ represents initial transactions initiated by chain j targeting chain ℓ within epoch t . Following intra-consensus validation, utilizing Eq.(3), this block becomes verified and is subsequently referred to as $\mathbf{Z}_{j,\ell}(t)$. Once $\mathbf{Z}_{j,\ell}(t)$ is submitted to the DAG and successfully passes inter-consensus verification, it is recorded as $\mathbf{Y}_{j,\ell}(t)$.

Remark 2: Concerning the ledger $\mathcal{Y}_j(t) = \bigcup_{\ell'=1}^{t-1} \mathbf{Y}_j^C(\ell')$ as introduced in Section 2.2.2, note that this collection comprises not only the confirmed transaction blocks $\{\mathbf{Y}_{j,\ell}(t')\}_{\ell=1}^N$ from chain j but also includes analogous blocks from other chains, specifically $\{\mathbf{Y}_{j',\ell}(t')\}_{\ell=1}^N$ for any $j' \neq j$. This aggregation ensures a comprehensive record of cross-chain transactions, facilitating a more robust and secure verification process across the network.

Next we define the cumulative matrices $\mathbf{W}_j^{in}(t)$ and $\mathbf{W}_j^{out}(t)$ as:

$$\mathbf{W}_j^{in}(t) = \sum_{r=1}^t \mathbf{A}_j(r), \quad \mathbf{W}_j^{out}(t) = \sum_{r=1}^t \mathbf{B}_j(r) + \mathbf{C}_j(t), \tag{2}$$

where $\mathbf{W}_j^{in}(t)$ represents the total inflow of tokens to chain j from other chains through epoch t , while $\mathbf{W}_j^{out}(t)$ summarizes the total outflow from chain j to other chains by epoch t . It should be noted that for $r = t$, $\mathbf{B}_j(t)$ represents the confirmed spending transactions for epoch t , whereas

$\mathbf{C}_j(t)$ does not include confirmed transactions. Instead, $\mathbf{C}_j(t)$ consists of proposed transactions that accounts on chain j intend to execute during epoch t .

A transaction involving account m in chain j during epoch t is deemed valid if the following condition is satisfied:

$$\begin{aligned} \mathbf{w}_j(t)[m] &= \sum_{m'=1}^M \mathbf{W}_j^{in}(t)[m', m] \\ &\quad - \sum_{m'=1}^M \mathbf{W}_j^{out}(t)[m, m'] \geq 0, \quad m = 1, \dots, M, \end{aligned} \quad (3)$$

where, $\mathbf{w}_j(t)[m]$ represents the net balance of account m at epoch t .

Then to compute the valid blocks $\mathbf{Z}_{j,\ell}(t)$ from each transaction block $\mathbf{X}_{j,\ell}(t)$, and consequently to obtain $\mathbf{Z}_j^P(t) = \{\mathbf{Z}_{j,\ell}(t)\}_{\ell=1}^N$, for each account m in chain j that $\mathbf{w}_j(t)[m] \geq 0$ we set $\mathbf{Z}_{j,\ell}(t)[m, m'] = \mathbf{X}_{j,\ell}(t)[m, m']$, and otherwise it is set to zero.

Remark 3: In SPID-Chain, in addition to $X_j^P(t)$, each chain j validates a subset of tip blocks during each epoch t . Specifically, it processes a set of K tip blocks, $\mathbf{Z}_j^T(t)$, using the operation $V_j^t(\mathbf{Z}_j^T(t), \mathcal{Y}_j(t)) = \mathbf{Z}_j^V(t)$ to produce the validated blocks $\mathbf{Z}_j^V(t)$. Each super-block $\mathbf{Z}_j^T(t)$ includes blocks $\mathbf{Z}_i^P(t_i)$ proposed by different chains $i \neq j$ at epoch $t_i \leq t$, with a restriction of including no more than one block from each chain.

For each block $\mathbf{Z}_i^P(t_i) = \{\mathbf{Z}_{i,\ell}(t_i)\}_{\ell=1}^N$ within $\mathbf{Z}_j^T(t)$, corresponding to (1) we denote:

$$\begin{aligned} \mathbf{A}_i(r) &= \sum_{\ell=1, \ell \neq i}^N \mathbf{Y}_{\ell,i}(r), \\ \mathbf{B}_i(r) &= \sum_{\ell=1, \ell \neq i}^N \mathbf{Y}_{i,\ell}(r), \quad r = 1, \dots, t, \\ \mathbf{C}_i(t) &= \sum_{\ell=1, \ell \neq i}^N \mathbf{Z}_{i,\ell}(t_i). \end{aligned} \quad (4)$$

Then chain j validates the K blocks $\mathbf{Z}_i^P(t_i)$ in $\mathbf{Z}_j^T(t)$ to obtain $\mathbf{Z}_j^V(t)$ by following the similar process for validating $X_j^P(t) = \{\mathbf{X}_{j,\ell}(t)\}_{\ell=1}^N$ as described by (2) and (3).

4.2 Coded Verification

4.2.1 Polar Encoding. We assume each chain j has n workers, and the probabilities $\{p_k\}_{k=1}^n$ of worker k being a straggler are given. Define $\lambda = \frac{1}{n} \sum_{k=1}^n p_k$. Then the rate of the Polar code is $R = 1 - \lambda$. Moreover, to describe the encoding process, we first form the set of stragglers \mathcal{S} consisting of worker nodes corresponding to the $|\mathcal{S}| = \lambda n$ highest values among $\{p_k\}_{k=1}^n$.

First assume that n is power of 2. To encode the $M \times M$ matrix $\mathbf{A}_j(r)$ in (1), its M rows are first evenly partitioned into $n(1 - \lambda)$ sets, and each resulting $\frac{M}{n(1-\lambda)} \times M$ submatrix is assigned to a non-straggler worker. And for a straggler worker in \mathcal{S} , a $\frac{M}{n(1-\lambda)} \times M$ all-zero matrix is assigned. This way an expanded matrix

$$\begin{aligned} \hat{\mathbf{A}}_j(r) &= \left[\mathbf{a}_{j,1}^\top(r) \quad \cdots \quad \mathbf{a}_{j,k}^\top(r) \quad \cdots \quad \mathbf{a}_{j,n}^\top(r) \right]^\top \\ &\in \mathbb{R}^{\frac{M}{1-\lambda} \times M} \end{aligned} \quad (5)$$

is obtained where $\mathbf{a}_{j,k}^\top(r)$ has dimension $\frac{M}{n(1-\lambda)} \times M$. If $k \in \mathcal{S}$ then it is an all-zero matrix, otherwise it is a submatrix of $\mathbf{A}_j(r)$.

Next an $n \times n$ Hadamard transform is applied to the $n \times 1$ block matrix in (5), resulting in the Polar coded matrix

$$\begin{aligned} \mathbb{H}_n\{\hat{\mathbf{A}}_j(r)\} &= \left[\tilde{\mathbf{a}}_{j,1}^\top(r), \dots, \tilde{\mathbf{a}}_{j,k}^\top(r), \dots, \tilde{\mathbf{a}}_{j,n}^\top(r) \right]^\top \\ &= \tilde{\mathbf{A}}_j(r) \in \mathbb{R}^{\frac{M}{1-\lambda} \times M}. \end{aligned} \quad (6)$$

where each $\tilde{\mathbf{a}}_{j,k}^\top(r)$ is a $\frac{M}{n(1-\lambda)} \times M$ non-zero matrix.

Next consider the case that n is not a power of 2. Then we can write $n = n_L + n_{L-1} + \dots + n_1$, where $n_L > n_{L-1} > \dots > n_1$ and each n_κ is a power of 2. For example, if $n = 100$, then $L = 3$, and $n_3 = 64$, $n_2 = 32$, and $n_1 = 4$.

Let $M_\kappa = \frac{n_\kappa}{n}M$, $\kappa = 1, \dots, L$. Then $M = M_L + \dots + M_1$. We divide the n worker nodes into L groups, with the κ -th group consist of n_κ worker nodes, and the corresponding straggler set \mathcal{S}_κ with $|\mathcal{S}_\kappa| = n_\kappa \lambda$.

The κ -th group encodes M_κ rows of the $M \times M$ matrix $\mathbf{A}_j(r)$ by first forming the corresponding expanded matrix $\hat{\mathbf{A}}_j^\kappa(r) \in \mathbb{R}^{\frac{M_\kappa}{1-\lambda} \times M}$ similar to (5), with n_κ row-blocks, and then applying an $n_\kappa \times n_\kappa$ Hadamard transform, resulting in Polar coded matrix $\tilde{\mathbf{A}}_j^\kappa(r) \in \mathbb{R}^{\frac{M_\kappa}{1-\lambda} \times M}$ similar to (6) with each row-block $\tilde{\mathbf{a}}_{j,k,\kappa}^\top(r)$ of dimension $\frac{M_\kappa}{n_\kappa(1-\lambda)} \times M$.

4.2.2 Coded Computing. Note that the uncoded computation in (2) can be written recursively as

$$\mathbf{W}_j^{in}(t) = \mathbf{W}_j^{in}(t-1) + \mathbf{A}_j(t), \quad (7a)$$

$$\mathbf{W}_j^{out}(t) = \mathbf{W}_j^{out}(t-1) + \mathbf{B}_j(t) + \Delta \mathbf{C}_j(t), \quad (7b)$$

where $\Delta \mathbf{C}_j(t) = \mathbf{C}_j(t) - \mathbf{C}_j(t-1)$. Correspondingly the coded versions of these updates are given by:

$$\tilde{\mathbf{W}}_j^{in}(t) = \tilde{\mathbf{W}}_j^{in}(t-1) + \tilde{\mathbf{A}}_j(t), \quad (8a)$$

$$\tilde{\mathbf{W}}_j^{out}(t) = \tilde{\mathbf{W}}_j^{out}(t-1) + \tilde{\mathbf{B}}_j(t) + \Delta \tilde{\mathbf{C}}_j(t). \quad (8b)$$

In the SPID-Chain, committee nodes, i.e., full nodes, are responsible for storing blocks in raw format. Worker nodes, on the other hand, manage coded data. In particular, assuming that n is a power of 2, each worker node k stores coded matrices:

$$\tilde{\mathbf{w}}_{j,k}^{in}(t) = \sum_{r=1}^t \tilde{\mathbf{a}}_{j,k}^\top(r), \quad \tilde{\mathbf{w}}_{j,k}^{out}(t) = \sum_{r=1}^t \tilde{\mathbf{b}}_{j,k}^\top(r) + \Delta \tilde{\mathbf{c}}_{j,k}^\top(t), \quad (9)$$

which correspond to the k -th row-block of the coded matrices in (8).

Then to compute (8a) and (8b) at each epoch t , SPID-Chain commences with full nodes encoding the current matrices $\mathbf{A}_j(t)$, $\mathbf{B}_j(t)$, and $\Delta \mathbf{C}_j(t)$ to obtain the encoded matrices $\tilde{\mathbf{A}}_j(t)$, $\tilde{\mathbf{B}}_j(t)$, and $\Delta \tilde{\mathbf{C}}_j(t)$ according to (6). Then with the help of some smart contracts committee nodes distribute the data $\tilde{\mathbf{a}}_{j,k}^\top(t)$, $\tilde{\mathbf{b}}_{j,k}^\top(t)$, and $\Delta \tilde{\mathbf{c}}_{j,k}^\top(t)$ to designated worker nodes. Upon receipt, each worker node updates its stored coded matrices by incorporating the new encoded data:

$$\tilde{\mathbf{w}}_{j,k}^{in}(t) = \tilde{\mathbf{w}}_{j,k}^{in}(t-1) + \tilde{\mathbf{a}}_{j,k}^\top(t), \quad (10a)$$

$$\tilde{\mathbf{w}}_{j,k}^{out}(t) = \tilde{\mathbf{w}}_{j,k}^{out}(t-1) + \tilde{\mathbf{b}}_{j,k}^\top(t) + \Delta \tilde{\mathbf{c}}_{j,k}^\top(t). \quad (10b)$$

Finally, worker nodes return the updated $\tilde{\mathbf{w}}_{j,k}^{in}(t)$ and $\tilde{\mathbf{w}}_{j,k}^{out}(t)$ to the committee nodes for decoding and obtaining (8a) and (8b), respectively, facilitated by a smart contract and an oracle. Specifically,

committee nodes assess whether the results received from worker nodes are decodable[48], i.e., if $\mathbf{W}_j^{in}(t)$ and $\mathbf{W}_j^{out}(t)$ can be reconstructed based on the received results from the worker nodes. Once confirmed as decodable, the committee nodes implement a recursive decoding algorithm [48, 49]. For details on the recursive decoding algorithm see Algorithms 1 and 2 in [48].

Remark 4: When n is not a power of 2, coded computing is carried out independently in L groups. In particular, within each group κ , the expressions in (7) now involve $\mathbf{W}_{j,\kappa}^{in}(t)$, $\mathbf{W}_{j,\kappa}^{out}(t)$, $\mathbf{A}_j^\kappa(t)$, $\mathbf{B}_j^\kappa(t)$, $\Delta\mathbf{C}_j^\kappa(t)$, while those in (8) involve $\tilde{\mathbf{W}}_{j,\kappa}^{in}(t)$, $\tilde{\mathbf{W}}_{j,\kappa}^{out}(t)$, $\tilde{\mathbf{A}}_j^\kappa(t)$, $\tilde{\mathbf{B}}_j^\kappa(t)$, and $\Delta\tilde{\mathbf{C}}_j^\kappa(t)$. Then, each worker node k in group κ stores coded matrices corresponding to (9), denoted as $\tilde{\mathbf{w}}_{j,k,\kappa}^{in}(t)$ and $\tilde{\mathbf{w}}_{j,k,\kappa}^{out}(t)$ which the procedure for updating these matrices are similar to (10) and are formed by the row-blocks $\tilde{\mathbf{a}}_{j,k,\kappa}^\top(t)$, $\tilde{\mathbf{b}}_{j,k,\kappa}^\top(t)$, and $\Delta\tilde{\mathbf{c}}_{j,k,\kappa}^\top(t)$, i.e., the k -th row-block of the encoded matrices $\tilde{\mathbf{A}}_j^\kappa(t)$, $\tilde{\mathbf{B}}_j^\kappa(t)$, and $\Delta\tilde{\mathbf{C}}_j^\kappa(t)$, respectively.

Moreover, the decoding process is also performed independently, in each group. Specifically, each worker node k in group κ sends back the intermediate values $\tilde{\mathbf{w}}_{j,k,\kappa}^{in}(t)$ and $\tilde{\mathbf{w}}_{j,k,\kappa}^{out}(t)$. Then, committee nodes decode these results to obtain the matrices $\mathbf{W}_{j,\kappa}^{in}(t)$ and $\mathbf{W}_{j,\kappa}^{out}(t)$. Once results are obtained for all L groups, the final $\mathbf{W}_j^{in}(t)$ and $\mathbf{W}_j^{out}(t)$ are formed.

Remark 5-motivation for coded computing: In case of uncoded computation each worker k stores an $\frac{1}{n}$ portion of matrices $\mathbf{A}_j(t)$, $\mathbf{B}_j(t)$, and $\Delta\mathbf{C}_j(t)$ as $\mathbf{a}_{j,k}^\top(t)$, $\mathbf{b}_{j,k}^\top(t)$, and $\Delta\mathbf{c}_{j,k}^\top(t)$, respectively, and computes $\mathbf{w}_{j,k}^{in}(t) = \sum_{r=1}^t \mathbf{a}_{j,k}^\top(r)$ and $\mathbf{w}_{j,k}^{out}(t) = \sum_{r=1}^t \mathbf{b}_{j,k}^\top(r) + \Delta\mathbf{c}_{j,k}^\top(t)$. Then during block verification, to obtain $\mathbf{W}_j^{in}(t)$ and $\mathbf{W}_j^{out}(t)$, as the system must wait for results from all workers, and therefore the slowest worker is the bottleneck. On the other hand, with coded computation, $\tilde{\mathbf{w}}_{j,k}^{in}(t)$ and $\tilde{\mathbf{w}}_{j,k}^{out}(t)$ are linear combinations of $\mathbf{a}_{j,k}^\top(t)$, $\mathbf{b}_{j,k}^\top(t)$, and $\Delta\mathbf{c}_{j,k}^\top(t)$ and such inherent redundancy ensures timely completion of the computation $\mathbf{W}_j^{in}(t)$ and $\mathbf{W}_j^{out}(t)$, even in the presence of slowest workers. Once the fastest workers complete their tasks, they send results back to the committee nodes, which then decode them without the need to wait for the slow workers.

Remark 6-motivation of Polar codes: Polar codes maintain a consistent error rate even as block lengths expand, ensuring efficient handling of both large and small computational tasks [50]. This consistent performance is crucial in Web3 scenarios, where tasks frequently involve managing varying amounts of data across multiple nodes, providing needed reliability and stability. Additionally, the encoding and decoding processes of Polar codes are less complex compared to other well-known codes like Reed-Muller or random linear codes [50]. This is particularly advantageous in Web3 networks, where quick data processing enhances system efficiency and resource optimization. Next we detail the structure of the smart contracts for token transferring.

4.3 Structure of the Smart Contracts for Token Transferring

For verifying token transfer transactions, we delineate the six blocks $\left\{C_j^k\right\}_{k=1}^6$ maintained by the committee nodes and their respective roles in each epoch t . The input, output, and state of each smart contract are denoted by $\left\{I_j^k(t), O_j^k(t), S_j^k(t)\right\}_{k=1}^6$, respectively.

4.3.1 Encoding and Decoding Processing Blocks. The initial two blocks, C_j^1 and C_j^2 , are allocated for encoding and decoding the *processing* block, respectively. To compute $P_j^t \left(X_j^P(t), \mathcal{Y}_j(t)\right) = Z_j^P(t)$, the smart contracts in these blocks are associated with the *defined major events* of forming $X_j^P(t)$ and computing the results of the worker to ascertain $Z_j^P(t)$, respectively.

a) *Encoding Processing Block*: C_j^1 is subscribed to the event published by the oracle resulting from the formation of block $X_j^P(t)$ by the committee nodes. Specifically, matrices $\mathbf{A}_j(t)$, $\mathbf{B}_j(t)$, and $\Delta\mathbf{C}_j(t)$ from (1) are formed by the committee nodes and provided to the oracle along with additional information such as the number of the worker nodes n and their public keys. Upon reception of such information, the oracle publishes an event, and upon its validation by committee nodes, it triggers C_j^1 .

- $I_j^1(t)$: Upon triggering, the input for C_j^1 serves as the encoder for the Polar code discussed in Section 4.2 This encoder initially forms the corresponding matrices $\hat{\mathbf{A}}_j(t)$, $\hat{\mathbf{B}}_j(t)$, and $\Delta\hat{\mathbf{C}}_j(t) = \hat{\mathbf{C}}_j(t) - \hat{\mathbf{C}}_j(t-1)$ using the information in the event published by the oracle as the result of the data provided by the committee nodes and then generates encoded matrices $\tilde{\mathbf{A}}_j(t)$, $\tilde{\mathbf{B}}_j(t)$, and $\Delta\tilde{\mathbf{C}}_j(t)$.
- $O_j^1(t)$: The output for C_j^1 comprises the set of computation tasks $\tilde{\mathbf{a}}_{j,k}^\top(t)$, $\tilde{\mathbf{b}}_{j,k}^\top(t)$, and $\Delta\tilde{\mathbf{c}}_{j,k}^\top(t)$ that are dispatched to each worker k .
- $S_j^1(t)$: After assigning the computation tasks to workers, the state of C_j^1 transitions to complete, and it utilizes an external entity to dispatch the assigned tasks to the workers.

b) *Decoding Processing Block*: C_j^2 is subscribed to the event published by the oracle as a consequence of receiving sufficient computation tasks from worker nodes. Thus, this smart contract corresponds to the *defined major event* of acquiring adequate computation results from worker nodes. Specifically, as delineated in Section 4.2, upon receiving enough decodable results from worker nodes, the oracle publishes an event and forwards this event to the committee nodes for verification and achieving consensus on its validity. Upon validation of the published event, it triggers C_j^2 . Each worker node k initially updates the stored encoded matrices $\tilde{\mathbf{w}}_{j,k}^{in}(t)$ and $\tilde{\mathbf{w}}_{j,k}^{out}(t)$ from (10) and transmits them back to the oracle in order to obtain (8a) and (8b), respectively.

- $I_j^2(t)$: The input for this smart contract leverages the computation results from workers and, firstly, utilizing the decoder embedded in C_j^2 obtains $\mathbf{W}_j^{in}(t)$ and $\mathbf{W}_j^{out}(t)$ in (7) and then verifies the transactions in $X_j^P(t)$ from (3).
- $O_j^2(t)$: With the verified transactions in $X_j^P(t)$, the output for C_j^2 is $Z_j^P(t)$, the proposed block for epoch t .
- $S_j^2(t)$: Upon successfully determining $Z_j^P(t)$, the state of C_j^2 transitions to complete.

4.3.2 *Encoding and Decoding Validation Blocks*. Blocks C_j^3 and C_j^4 in the SPID-Chain function similarly to the initial encoding and decoding blocks, C_j^1 and C_j^2 , but are specifically designed to handle multiple tip blocks on the DAG.

a) *Encoding Validation Block*: C_j^3 , the encoding validation block, parallels the operations of C_j^1 but is triggered for each $Z_i^P(t_i)$ in $\mathbf{Z}_j^T(t)$, for $t_i \leq t$ at the tip of the DAG, repeating the process for each block, up to a total of K blocks. C_j^3 processes input similarly to C_j^1 , but it applies the encoding operations to multiple blocks from different chains, each represented once among the tip blocks to obtain $\tilde{\mathbf{A}}_i(t)$, $\tilde{\mathbf{B}}_i(t)$ and $\Delta\tilde{\mathbf{C}}_i(t)$, refer to (4) for each block $Z_i^P(t_i)$ in $\mathbf{Z}_j^T(t)$.

b) *Decoding Validation Block*: Similarly, C_j^4 , the decoding validation block, mirrors C_j^2 's functionality but extends it to handle multiple blocks at the DAG's tip. It is triggered upon receiving result of the computation tasks $\tilde{\mathbf{w}}_{i,k}^{in}(t)$ and $\tilde{\mathbf{w}}_{i,k}^{out}(t)$ for each of these blocks, ensuring that the decoding and validation processes are executed repetitively for up to K blocks.

Upon successfully determining valid transaction in $Z_i^P(t_i)$ for all blocks in $Z_j^T(t)$, block $Z_j^V(t)$ is determined.

4.3.3 Submission Block. Block C_j^5 is designated as the *submission* block. The smart contract within this block is utilized in SPID-Chain to submit the block $Z_j^P(t)$ to the DAG. As discussed in Section 3.2.1, the smart contract in this block corresponds to the *defined major event* of forming $Z_j^V(t)$. Specifically, C_j^5 is *subscribed* to the event *published* by the oracle resulting from the formation of block $Z_j^V(t)$ by the committee nodes. When block $Z_j^V(t)$ is formulated by the committee nodes and provided to the oracle, it publishes an event that, upon validation, triggers C_j^5 .

- $I_j^5(t)$: Upon triggering, the input $I_j^5(t)$ for C_j^5 it identifies the valid blocks within $Z_j^V(t)$ on the DAG. Considering that the vertices corresponding to blocks in $Z_j^V(t)$ serve as the parents for $Z_j^P(t)$, the function embedded in C_j^5 updates the AW of the vertices on the DAG.
- $O_j^5(t)$: Consequently, the output of C_j^5 alters the status of those blocks in the DAG whose AW exceeds a predetermined threshold from *proposed* to *confirmed*.
- $S_j^5(t)$: After successfully obtaining the output of C_j^5 , the state of C_j^5 releases the proposed block $Z_j^P(t)$ for epoch t into the DAG by creating a new vertex. This vertex establishes directed edges to vertices representing the parent blocks in $Z_j^V(t)$, which contain the valid blocks.

4.3.4 Updating Block. C_j^6 is designated as the *updating* block. The smart contract within this block is utilized in SPID-Chain to form $Y_j^C(t+1)$ and consequently update the ledger to ascertain $\mathcal{Y}_j(t+1)$. As discussed in Section 3.2.1, the smart contract in this block corresponds to the *defined major event* of forming super-block $Y_j^C(t+1)$. Specifically, C_j^6 is *subscribed* to the event *published* by the oracle resulting from the formation of block $Y_j^C(t+1)$ by the committee nodes. To form $Y_j^C(t+1)$ committee nodes in chain j take only one block from those chains that have at least one block. Then, upon providing the block $Y_j^C(t+1)$ to the oracle, it publishes an event that, upon validation, triggers C_j^6 .

- $I_j^6(t)$: Upon triggering, the input for C_j^6 incorporates the transaction into $\mathcal{Y}_j(t+1)$ using the information in the event, which essentially comprises the confirmed transactions in $Y_j^C(t+1)$.
- $O_j^6(t)$: As a consequence of the input, the output of C_j^6 yields the ledger $\mathcal{Y}_j(t+1)$, which is maintained by the committee nodes and is utilized for the subsequent epoch.
- $S_j^6(t)$: After successfully determining $\mathcal{Y}_j(t+1)$, the state of C_j^6 transitions to complete.

Table. 3 summarizes the structure of the smart contracts for token transferring.

4.4 Stages of SPID-Chain

For each set of six smart contracts, $\{C_j^i\}_{i=1}^6$, triggered by a confirmed even, i.e., an event that has been validated through consensus by the committee nodes—we denote the confirmed event as $\mathcal{X}_j^i(t)$. This event triggers the corresponding smart contracts $\{C_j^i\}_{i=1}^6$ in epoch t . Furthermore, we denote by \mathcal{T}_j a temporary pool consisting of events $\mathcal{X}_j^i(t)$. This pool is populated at the start of each epoch t and is emptied at the epoch's end, following the completion of all stages in the SPID-Chain's protocol, and its contents are recorded in a block denoted by $\mathcal{D}_j(t)$ which is the t -th block in the side event ledger \mathcal{D}_j . Therefore, the operation of SPID-Chain network is driven by a sequence of stages, executed by each chain j in every epoch t . These stages are:

Stage 1: Proposed Block Generation:

Table 3. Summary of Smart Contracts for Token Transferring

Block	Major Defined Event Subscription	Input	Output	State
C_j^1	Formation of $X_j^P(t)$	Encoder using matrices $\hat{A}_j(t)$, $\hat{B}_j(t)$, $\Delta\hat{C}_j(t)$	Set of computation tasks $\hat{a}_{j,k}^\top(t)$, $\hat{b}_{j,k}^\top(t)$, $\Delta\hat{c}_{j,k}^\top(t)$	Complete after dispatching tasks to the workers
C_j^2	Receiving enough computation results	Leveraging computation results from workers to decode and verify transactions	Proposed block for epoch t , $Z_j^P(t)$	Complete after finding $Z_j^P(t)$
C_j^3	Formation of $Z_j^T(t)$	Encoder using matrices $\hat{A}_i(t)$, $\hat{B}_i(t)$, $\Delta\hat{C}_i(t)$	Set of computation tasks for worker nodes	Complete after dispatching tasks to the workers
C_j^4	Receiving enough computation results	Utilizing computation results from workers to decode and verify blocks	Validated transactions in $Z_i^P(t_i)$	Complete after finding $Z_j^V(t)$
C_j^5	Formation of $Z_j^V(t)$	Identifying valid blocks in $Z_j^V(t)$ on the DAG	Updating AW and changing status of blocks in DAG from <i>proposed</i> to <i>confirmed</i>	Releases the proposed block $Z_j^P(t)$ into the DAG
C_j^6	Formation of $Y_j^C(t+1)$	Adding transactions to $Y_j(t+1)$	Ledger $Y_j(t+1)$	Complete after updating the ledger

Step 1: Computation tasks for computing P_j^t are assigned to the workers: Following committee-committee consensus block $X_j^P(t)$ is formed and submitted to the oracle. As a result, an event is published consisting of block $X_j^P(t)$, which is validated by nodes in $C_j(t)$. After reaching consensus for a valid event $X_j^1(t)$, it is added to pool \mathcal{T}_j . As a result, the smart contract in encoding processing block C_j^1 is activated, assigning computation tasks to their corresponding worker nodes.

Step 2: Worker nodes perform the computations and send the results to the oracle: Each worker node k performs the computations and submits the results to the oracle.

Step 3: Decoding the computation results and obtaining the proposed block: Upon receiving the computation results from the worker nodes, the oracle publishes an event that includes these results. Subsequently, the nodes within $C_j(t)$ utilize committee-committee consensus to agree on a valid event, denoted as $X_j^2(t)$. This event triggers the smart contract in the decoding processing block C_j^2 . The event $X_j^2(t)$ is then added to the pool \mathcal{T}_j . The addition of $X_j^2(t)$ to \mathcal{T}_j activates the smart contract in C_j^2 , leading to the generation of the proposed block $Z_j^P(t)$, which is subsequently added to the oracle.

Stage 2: Validation of Tip Blocks on DAG:

Step 1: Computation tasks regarding validating tip blocks on the DAG are assigned to the workers: Nodes in $C_j(t)$ first create a super-block $Z_j^T(t)$ from the tip blocks on the DAG and submit this to the oracle. Subsequently, an event containing the super-block $Z_j^T(t)$ is published. The nodes then reach a consensus on a valid event, labeled as $X_j^3(t)$, which triggers the smart contract in the encoding validation block C_j^3 upon its addition to the pool \mathcal{T}_j . Following this, the computation tasks assigned are dispatched to their respective worker nodes.

Step 2: Worker nodes perform the computations and send the results to the oracle: Each worker node k performs the computations and submits the results to the oracle.

Step 3: Decoding the computation results and obtaining the valid super-block: The oracle collects the computation results from the worker nodes and publishes an event encapsulating these results. Utilizing the committee-committee consensus, nodes in $C_j(t)$ reach consensus on an event, denoted as $X_j^4(t)$. This event activates the smart contract in the decoding validation block C_j^4 when is added to pool \mathcal{T}_j . As a result, a validated super-block $Z_j^V(t)$, comprising the set of valid blocks within $Z_j^T(t)$, is obtained and subsequently added to the oracle.

Stage 3: Proposed Block Submission and AW Updating:

Step 1: Submission of the proposed block: With $Z_j^P(t)$ as the proposed block from Stage 1 and $Z_j^V(t)$ as the valid super-block from Stage 2, the oracle publishes an event. This event is validated by nodes in $C_j(t)$ following the committee-committee consensus. The consensus-validated event, denoted as $X_j^5(t)$, is added to the pool \mathcal{T}_j , triggering the smart contract in the submission block C_j^5 . Subsequently, the proposed block $Z_j^P(t)$ is submitted to the DAG, creating a new vertex. This vertex establishes directed edges to vertices representing parent blocks in $Z_j^V(t)$, encompassing the valid blocks.

Step 2: Adding the received proposed blocks from other blockchains to the DAG: The oracle monitors and publishes an event about the latest blocks added to the DAG by other blockchains. The committee nodes validate this event. Upon validation, triggering the smart contract it adds $Z_{j'}^P(t)$, the proposed blocks from other blockchains j' , to the DAG copy for D_j .

Step 3: Updating the AW of blocks on DAG: Following the committee-committee consensus, nodes in $C_j(t)$ agree on a valid event, $X_j^6(t)$, published by the oracle. This event concerns the update of the AW of blocks on the DAG. The event $X_j^6(t)$ is added to \mathcal{T}_j . It activates the smart contract C_j^5 , facilitating the update of the AW of the blocks on the DAG and their corresponding status.

Stage 4: Updating the ledger:

Step 1: Updating chain $\mathcal{Y}_j(t)$: Nodes in $C_j(t)$ create the super-block $Y_j^C(t+1)$ from the confirmed blocks on the DAG and then submitted it to the oracle. Following this submission, an event is published. The nodes then reach a consensus on a valid event, denoted as $X_j^7(t)$, which triggers the smart contract in the updating block C_j^6 upon its addition to the pool \mathcal{T}_j . Then confirmed super-block $Y_j^C(t+1)$ is added to chain \mathcal{Y}_j , resulting in the updated chain $\mathcal{Y}_j(t+1)$ which is stored by the committee nodes.

Step 2: Updating event chain \mathcal{D}_j : Committee nodes store the ledger $Y_j^C(t+1)$ and remove the pool of temporary events in \mathcal{T}_j . The set of these removed events is then added to the side event ledger \mathcal{D}_j as the block $\mathcal{D}_j(t)$.

5 SIMULATIONS

This section provides a thorough simulation study of our proposed SPID-Chain system to showcase its excellent performance in terms of throughput and scalability, decentralization, latency and DAG expansion rate, and resistance to double-spending attack.

5.1 Simulation Setup

To simulate our SPID-Chain system, we employed Substrate [51], a modular framework for building blockchains, to define individual blockchains with distinct consensus mechanisms. These blockchains operate independently while being capable of intercommunication through custom bridging solutions which in our scheme is the DAG ledger. For the DAG structure, we utilized Docker [52] to create a controlled virtual environment, deploying multiple GoShimmer [53] node instances as our blockchains using Docker Compose. This setup allowed us to simulate a network with behavior closely resembling real-world conditions, with the flexibility to adjust parameters as needed. The integration between the Substrate-defined blockchains and the DAG was achieved through a custom-built bridge module, implemented in Rust [54], the primary programming language used for Substrate development. This module utilized Substrate's extensible architecture to facilitate communication between the blockchains and the DAG. Additionally, the Go programming language was employed to interface with the GoShimmer nodes of the DAG, leveraging Go's robust networking capabilities. The bridge module acted as a translator, converting the data formats and consensus signals between the Substrate blockchains and the IOTA-based DAG. This allowed for

seamless interoperability, ensuring that transactions could be validated and processed across the different systems without compatibility issues.

In each blockchain we set the number of the committee nodes as $\frac{n}{10}$, where n is the number of worker nodes in each blockchain. Specifically, we employed the libsodium [55] cryptographic library to implement the verifiable random function (VRF) within our Substrate-based blockchains. Each committee node generates a VRF output using its private key and a shared random seed, synchronized across the network using the network time protocol (NTP) to ensure consistent epoch times. The seed is distributed securely to all nodes at the start of each epoch through a decentralized broadcast protocol.

In the simulations, honest blockchains adhere to both intra- and inter-consensus protocols. In particular, during Stage 3, they follow established guidelines for selecting parent blocks and issuing valid blocks. We denote the per-minute block issuance rate by honest blockchains during this stage as γ_h . On the other hand, adversarial blockchains follow the intra-consensus protocol but deviate during Stage 3 by consistently issuing invalid blocks. Moreover, in selecting parent blocks, adversarial blockchains adopt the *orphanage attack* strategy that involves choosing a parent with the oldest possible generation age and, when feasible, prioritizing their own blocks at the DAG's tip. We denote the per-minute block issuance rate by adversarial blockchains during Stage 3 as γ_a .

Consequently, the total block issuance rate per minute of the DAG is given by $\gamma = \gamma_a + \gamma_h$, and the spamming rate of the adversarial blockchains is defined as $\mu = \frac{\gamma_a}{\gamma}$. The critical spamming rate is defined as $\mu_{\text{crit}} = \frac{K-1}{K}$, where K is the number of blocks selected for processing in Stage 3 of the protocol. If $\mu > \mu_{\text{crit}}$ then the tip pool size grows rapidly with μ , as demonstrated in [57] for the IOTA-type DAG ledger.

Each simulation runs for a duration of 5 minutes, during which 500 blocks are generated at a rate of $\gamma = 100$ blocks per minute. These blocks are subsequently attached to the DAG.

Additionally, for a given value λ , we randomly select λn worker nodes to form the set of stragglers \mathcal{S} . A straggler never returns any results while if a node is not a straggler, it always returns the computation results correctly and on time.

We utilized the BigQuery [56] public Ethereum dataset to obtain samples of real-world blockchain transactions. To generate invalid blocks, we modified the account balances in a subset of transactions so that they exceed the maximum allowable balance. These altered transactions were then grouped with unmodified, valid transactions to form invalid blocks. In our simulation, while a valid block contains just valid transactions, each invalid block contains a mixture of valid and invalid transactions. We set the number of accounts in each blockchain to $M = 1000$. Moreover, for each simulation, 20% of the blockchains are designated as adversarial with varying spamming rate.

Finally, each result is the average of 10 runs. We set both the task completion timeout for workers and voting timeout for committee nodes to 500 milliseconds, with a round stage occurring when all tasks are completed. The epoch transition happens when nodes in a blockchain have processed the entire task list. We also set the bandwidth to 20 Mbps and imposed a latency of 100 ms on all communication links in all simulations.

5.2 Results

5.2.1 Throughput and Scalability. In this section, we will investigate the throughput and scalability of our proposed scheme, focusing on two distinct aspects: intra-consensus and inter-consensus. Throughput is a critical metric that assesses the speed and accuracy with which blocks are processed within a system. Scalability, on the other hand, is an essential factor in determining a system's capacity to manage growing workloads while maintaining efficient performance.

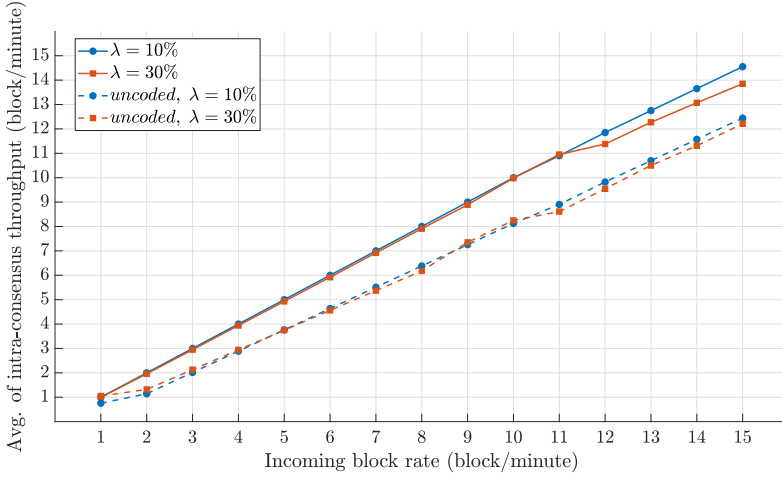


Fig. 2. Intra-consensus throughput with $N = 10$, $n = 100$, and for varying straggler worker percentages λ and incoming block rates.

Intra-consensus throughput: Intra-consensus throughput is defined as the average number of blocks processed by a scheme per minute. The intra-consensus throughput focuses on the processing speed and accuracy of blocks within each individual blockchain. To measure intra-consensus throughput, we calculate the *average* number of blocks correctly generated by honest blockchains within the network per minute. Notably, the intra-consensus throughput remains unaffected by the spamming rate of adversarial blockchains, as blocks from these sources are deemed invalid and thus excluded from the calculations. Furthermore, since blocks generated by honest blockchains are always considered valid, there is no need to assess the accuracy of these blocks.

In our throughput simulations, we define a block as processed once its AW exceeds 67% and it's confirmed. We set up $N = 10$ blockchains, each with $n = 100$ worker nodes, varying the percentage of stragglers $\lambda \in \{10\%, 30\%\}$ and the rate of incoming blocks. Our findings, illustrated in Fig. 2, show that blockchains using the SPID-Chain scheme process transactions up to 11 blocks per minute before the slope of the throughput begins slightly to decline, particularly at a higher straggler rate of 30%. In contrast, networks without encoding experience a steady decline in throughput.

Moreover, intra-consensus throughput is generally lower in networks without encoding. The use of Polar encoding in SPID-Chain helps distribute computations across nodes, mitigating the negative impact of stragglers by offloading tasks to faster workers. This efficiency, however, comes at the cost of increased data transmission bandwidth between committee and worker nodes.

Intra-consensus scalability: Intra-consensus scalability refers to a blockchain system's ability to increase the number of nodes within each blockchain and it is illustrated in terms of the intra-consensus versus the number of nodes in each blockchain. By setting incoming block rates at 12 blocks per minute with $\lambda = 10\%$, and varying the number of blockchains $N \in \{5, 15\}$, the system demonstrates how scalability is affected by node count. Fig. 3 shows the intra-consensus scalability. Systems using the Polar encoding scheme successfully manage the addition of the worker nodes, by improving work distribution among the worker nodes. In contrast, systems lacking encoding experience a decrease in throughput as more nodes lead to slower computations and extended protocol stages.

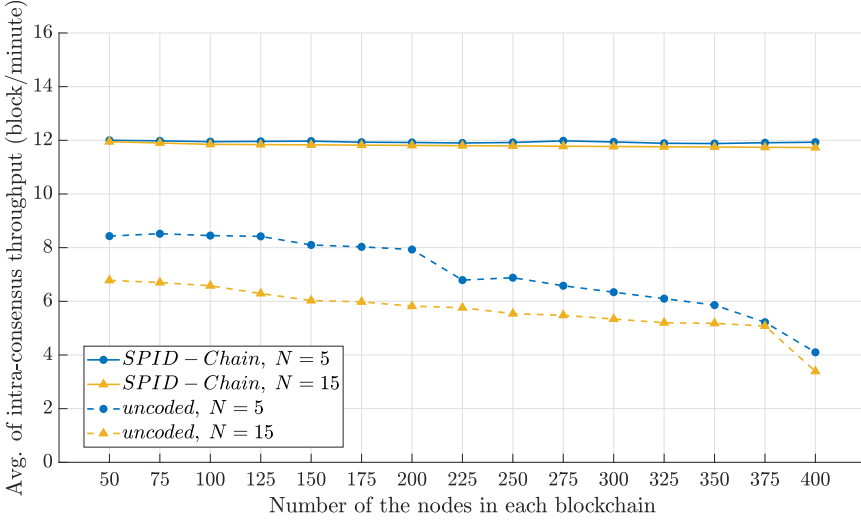


Fig. 3. Intra-consensus scalability with $\lambda = 10\%$, 12 blocks per minute for rate of incoming blocks, and for varying numbers of nodes within each blockchain and different numbers of blockchains N .

Inter-consensus throughput: The inter-consensus throughput measures the rate at which blocks are processed on the DAG ledger. For evaluating the inter-consensus throughput, it is crucial to consider both the accuracy, which indicates the correctness of decisions made during block processing on the DAG, and the time required for processing blocks. Therefore, we count the number of the correctly confirmed blocks on the DAG per minute.

Figure 4 illustrates the inter-consensus throughput with settings of $\lambda = 10\%$, $K = 2$, resulting in a critical spamming rate $\mu_{\text{crit}} = 50\%$, and varying spamming rates $\mu \in \{10\%, 55\%\}$. Throughput improves as the rate of incoming blocks increases, leveraging the DAG structure where new blocks increase the AW of existing ones, thereby facilitating faster confirmation. This mechanism underscores the strength of DAG-based ledgers in scaling confirmation and processing speeds. Notably, at a low spamming rate of $\mu = 10\%$, throughput significantly rises as the block rate exceeds 8 per minute. On the other hand, at $\mu = 55\%$, despite still experiencing an increase, throughput growth is less pronounced due to adversarial actions that modify the DAG’s structure, leading to fewer correct block confirmations. Nonetheless, even under higher spamming conditions of $55\% = \mu > \mu_{\text{crit}}$, SPID-Chain shows an overall throughput increase.

Similarly, for the systems using dashed lines where encoding is absent, we observe the same trend of increased throughput with a rising rate of incoming blocks. However, this effect is much less pronounced compared to systems with Polar encoding, to the extent that it diminishes the advantages of using a DAG ledger. Specifically, the use of Polar encoding enables honest blockchains to process blocks more efficiently by distributing the workload, which helps them counteract the spamming tactics of adversarial nodes. Specifically, in Stages 1 and 2 of the SPID-Chain, the implementation of distributed coding accelerates the processing of each honest blockchain’s proposed block and the tip blocks on the DAG. This acceleration is evident in Stage 3, where it significantly enhances the inter-consensus throughput. The faster selection and processing of the proposed block and its parents from Stages 1 and 2 allow for quicker submissions to the DAG in Stage 3, thereby increasing the inter-consensus throughput.

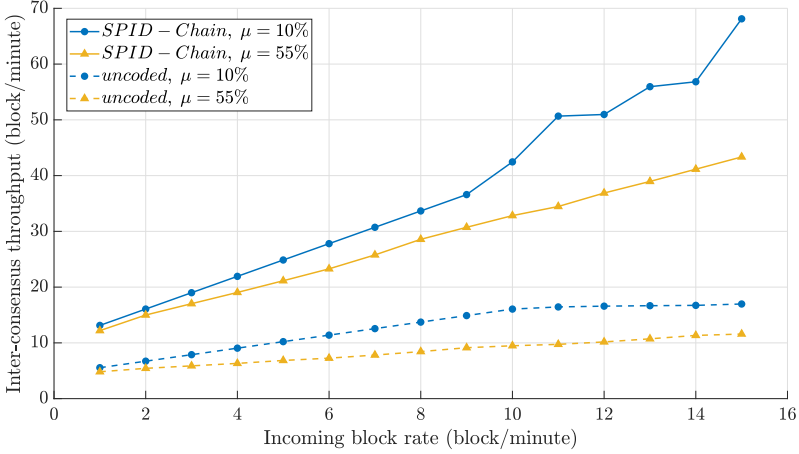


Fig. 4. Inter-consensus throughput with $\lambda = 10\%$, $N = 10$, $K = 2$, $\mu_{\text{crit}} = 50\%$, and for varying rates of incoming blocks and spamming rates.

In contrast, without encoding, it takes longer to process blocks and attach them to the DAG, allowing adversarial blockchains to attach their blocks more strategically, leading to the confirmation of more invalid blocks and, therefore, lowering the accuracy.

Inter-consensus scalability: Inter-consensus scalability pertains the ability of a system to handle an increased number of interconnected blockchains within a DAG structure, crucial for managing more blocks across multiple blockchains. We maintained a constant block arrival rate of 10 blocks per minute with specific parameters $\mu = 20\%$, $\lambda = 10\%$, $K = 2$, $\mu_{\text{crit}} = 50\%$, $\eta = 67\%$ and varied both the number of blockchains N and the worker nodes per blockchain $n \in \{100, 200\}$.

Figure 5 illustrates the inter-consensus scalability of the SPID-Chain. As depicted, the system’s performance improves with the addition of more blockchains, marked by increased inter-consensus throughput. This enhancement is due to the faster accumulation of blocks within the DAG and the accelerated AW of these blocks, which expedites the confirmation process a key feature of DAG-based ledgers. However, for the solid lines represent the SPID-Chain model utilizing Polar encoding it is observed that as the number of nodes within each blockchain rises, so does the system’s throughput. This improvement is largely because Polar encoding streamlines the block processing and distribution of computational tasks among nodes, making the system more efficient. On the other hand, the dashed lines represent systems without encoding. Here, although throughput increases with more blockchains, the rise is less marked. This suggests that networks lacking encoding fail to fully leverage the inherent scalability benefits of DAG ledgers. The longer processing times result in fewer blocks being attached to the DAG, compromising the ledger’s scalability advantage. Moreover, in systems without encoding, increasing the number of worker nodes does not enhance throughput but instead decreases it, due to longer times required to compile results, complete computations, achieve consensus, and process blocks.

5.2.2 Decentralization. In the context of blockchain interoperability and DAG-based ledger systems, decentralization is a crucial aspect that extends beyond mere block throughput. It is essential to consider the distribution of confirmed blocks across the DAG, as a system with high throughput but concentrated block confirmations among a subset of blockchains may not truly embody the decentralized ethos of blockchain technology. A scheme that ensures a more uniform distribution

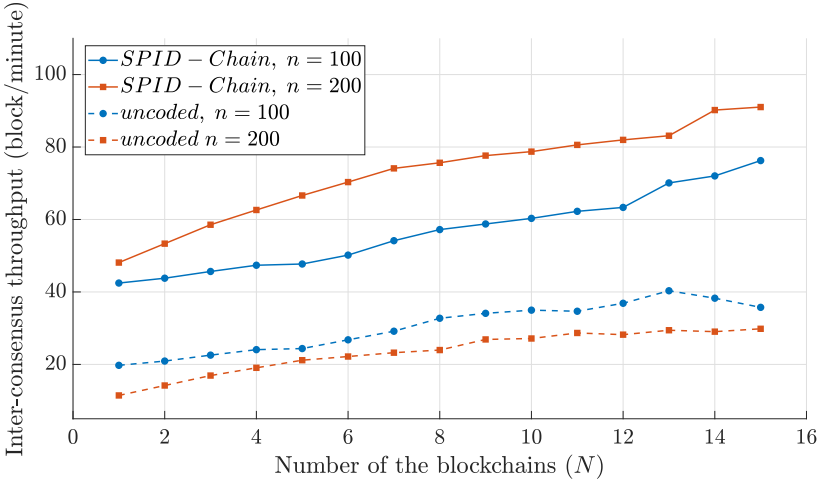


Fig. 5. Inter-consensus scalability for varying numbers of blockchains N and worker nodes within each blockchain $n \in \{100, 200\}$ with fixed incoming block rate 10 blocks per min, $\mu = 20\%$, $\lambda = 10\%$, $K = 2$, and $\mu_{\text{crit}} = 50\%$.

of confirmed blocks across participating blockchains fosters a more resilient and decentralized network, reducing the risk of centralization and the potential for collusion among a few dominant blockchains.

We employ the Gini coefficient [58] as a measure of the decentralization of our network. The Gini coefficient is defined as:

$$I(t) = \frac{\sum_{i=1}^N \sum_{j=1}^N |\phi_i(t) - \phi_j(t)|}{2N \sum_{j=1}^N \phi_j(t)}. \quad (11)$$

Here, $\phi_j(t)$ represents the number of blocks confirmed by chain j at epoch t . Smaller variations among $\phi_j(t)$ result in a lower Gini coefficient, indicating better decentralization, as it implies a more even distribution of block confirmations across the network. As measured in [58], the Gini coefficients for the Bitcoin and Ethereum networks average 0.8 and 0.5, respectively. These two blockchains, known as dominant and widely recognized benchmarks, can serve as standards for evaluating the decentralization performance of various schemes.

We simulate our scheme for different values of K and varying the spamming rate μ of the adversarial. For all cases, we set $N = 10$, $n = 100$, and $\lambda = 10\%$. Fig. 6 shows the decentralization of SPID-Chain. As we see for all the different cases and scenarios the proposed scheme shows good decentralization comparing to the Gini coefficients of Bitcoin and Ethereum. Moreover, as the parameter K increases, there is a corresponding decrease in the maximum Gini coefficient across the bins in each subplot, suggesting an enhancement in the decentralization of the network. Specifically, for each value of K , when the spamming rate μ surpasses the critical threshold (μ_{crit}), decentralization begins to deteriorate as evidenced by an increasing Gini coefficient. However, as K increases, this degradation becomes progressively less pronounced.

The reason is the system's ability to validate more blocks through honest blockchains, which in turn select a greater number of parents for the blocks they add to the DAG K , effectively counters the orphanage strategy employed by adversarial blockchains. This strategy typically involves adversarial blockchains preferentially attaching their blocks to previous blocks of their own making. Our simulations demonstrate that increased K values mitigate this behavior, leading to a more

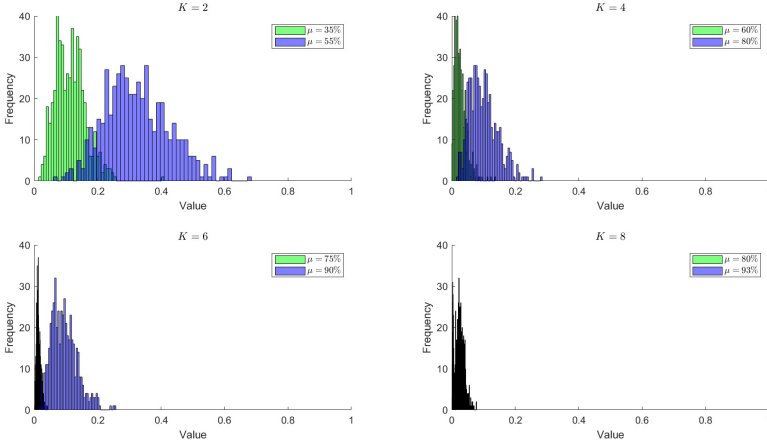


Fig. 6. Network decentralization measured by Gini coefficient for different K and μ_{crit} values and spamming rates (μ), with $N = 10$, $n = 100$, and $\lambda = 10\%$.

decentralized and secure network that upholds the integrity of the ledger against such adversarial tactics.

5.2.3 Security.

Latency and DAG expansion rate: In the domain of blockchain interoperability, the two primary metrics of importance are the inter-chain block finality time and the DAG expansion rate, which basically is the evolution of the tip pool size over the time.

Inter-chain block finality time is critical for assessing the latency in cross-chain transactions, indicating the time it takes for a block to be irreversibly recorded on the DAG ledger. A shorter finality time suggests a faster system, which is crucial for user experience and the swift settlement of transactions.

The DAG expansion rate provides insights into the network’s structural growth by measuring how quickly the DAG’s tip pool size increases with contributions from various blockchains. This rate is key to understanding the network’s activity level and its ability to scale efficiently. Proper management of the tip pool size is vital to avoid congestion and maintain transaction processing efficiency, which in turn ensures the network’s security.

For an effective DAG ledger, the size of the tip pool should remain relatively stable and small over time, showing less sensitivity to the spamming rates imposed by adversarial blockchains. An increase in the tip pool size reduces the likelihood of blocks at the tip being selected for validation, thereby extending the time to finality. In scenarios where the tip pool size grows exponentially—referred to as over-inflation—it leads to a higher probability of blocks becoming orphaned, as discussed in [59].

To assess the latency and DAG expansion rate, i.e., tip pool size, in our system, as well as to explore the impact of the critical point, we simulated a network consisting of $N = 10$ blockchains, each with $n = 100$ worker nodes. Among these nodes, $\lambda = 10\%$ were identified as stragglers. We set $\eta = 67\%$ and tested two settings: $K = 2$ with $\mu \in \{35\%, 55\%\}$ and $K = 4$ with $\mu \in \{60\%, 80\%\}$. This span covers both below and above the critical spamming rates of $\mu_{\text{crit}} = 0.5$ for $K = 2$ and $\mu_{\text{crit}} = 0.75$ for $K = 4$.

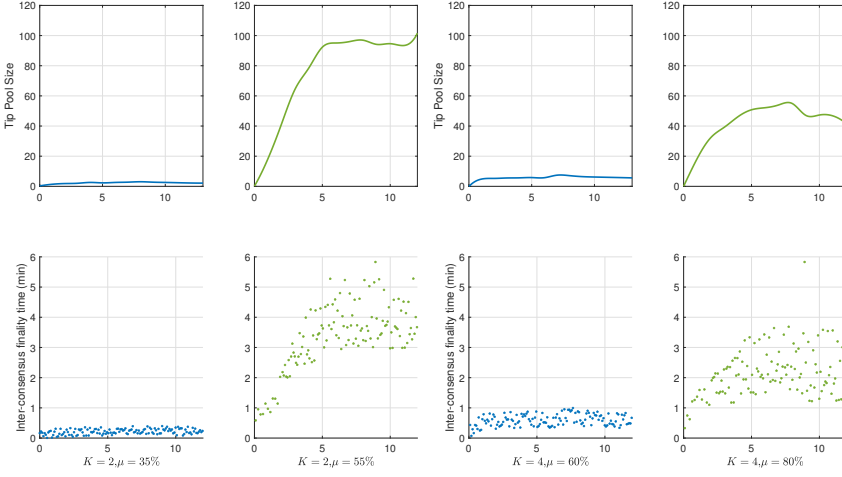


Fig. 7. Impact of varying spamming rate (μ) on DAG ledger health, demonstrated by tip pool size and inter-chain block finality time. Simulation parameters: $N = 10$ blockchains, $n = 100$ worker nodes with $\lambda = 10\%$, $\eta = 67\%$, $K = 2$, $\mu_{\text{crit}} = 50\%$ and $\mu \in \{35\%, 55\%\}$, $K = 4$, $\mu_{\text{crit}} = 75\%$ and $\mu \in \{60\%, 80\%\}$.

For each μ value, the network operated for 12 minutes, during which we monitored the confirmation status of blocks on the DAG. Fig. 7 illustrates the tip pool size and provides a scatter plot of the inter-chain block finality times. Results show that higher μ values lead to an increased tip pool size and longer confirmation times for blocks. Notably, with both $K = 2$ and $K = 4$, the tip pool size and inter-chain block finality times exhibit increased vulnerability when $\mu > \mu_{\text{crit}}$, as evidenced by an expansion in the tip pool size and extended finality times for the blocks. However, as shown in Fig. 7 for $K = 4$, the adverse effects on the tip pool size and finality times are less severe when μ exceeds μ_{crit} . Therefore, it is recommended that for enhanced DAG ledger health and reduced finality times, larger values of K should be considered.

Double Spend Resistant Analysis: In blockchain systems, a double spend attack refers to a scenario where an attacker successfully spends the same digital currency or asset twice. This type of attack exploits vulnerabilities in the network’s consensus mechanism or propagation delays to manipulate transaction records.

To simulate double-spend scenarios within our SPID-Chain framework, we devised a specific method for creating double-spend blocks. Each double-spend block was constructed to contain transactions that are valid in isolation—meaning the sender possesses adequate tokens for the transaction, thus each transaction adheres to standard validation protocols. However, the double-spend characteristic was introduced by replicating the same transaction, with identical signatures and identifiers, across two different blocks. Specifically, among the 100 double-spend blocks prepared for the simulation, we organized these into 50 pairs, with each pair containing one replicated transaction while maintaining unique non-duplicate transactions in the remainder of the blocks.

To integrate these double-spend blocks into our network simulation, we attached 100 double-spend blocks at random points within the DAG, in addition to the 300 regular blocks. This approach created a diverse tip pool that included both double-spend and regular transaction blocks. The detection mechanism within the SPID-Chain was tasked with identifying and labeling the double-spend transactions based on discrepancies observed in the transaction records across the DAG

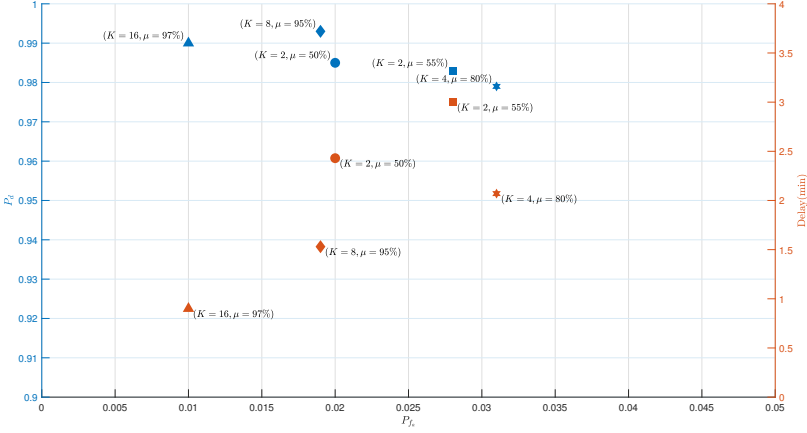


Fig. 8. Performance of SPID-Chain in detecting double-spend blocks with $N = 10$, $\lambda = 10\%$, and $\eta = 67\%$.

by the committee nodes. Specifically, In Stage 2, committee nodes while assembling the super-block $Z_j^T(t)$ during an epoch t , exclude any double-spend blocks detected. Upon submitting their proposed block $Z_j^P(t)$ to the DAG in Stage 3, they label any double-spend blocks within $Z_j^T(t)$. A double-spend block is considered detected once the block $Z_j^P(t)$ is confirmed as $Z_j^C(t)$.

We set $N = 10$, $\lambda = 10\%$, $\eta = 67\%$, and varied the spamming rate of adversaries, μ , and the number of blocks selected for processing from the tip pool, K . The probability of false alarm, P_{fa} , is defined as the percentage of regular blocks mistakenly identified as double-spend blocks. Conversely, the probability of detection, P_d , refers to the percentage of correctly identifying actual double-spend blocks. We also measured the speed of identification as the delay where we measure after all the 400 blocks are processed.

The results, displayed in Fig. 8, demonstrate that the SPID-Chain effectively identifies double-spend blocks across all K values with a low P_{fa} . Larger K values slightly increase P_d and reduce identification delays, which aligns with expectations as processing more blocks per chain increases detection chances and speed.

It is crucial to note the simulation also accounted for adversaries operating above the critical spamming rate, significantly challenging the DAG's topology and the process of invalidating double-spend attacks. Despite this, SPID-Chain effectively resisted the attacks. For instance, at $K = 2$ and $\mu = 55\%$, despite the longer detection time compared to the critical spamming rate of $\mu = 50\%$, the system still managed to detect double-spend blocks efficiently with acceptable delays.

6 CONCLUSION

The proposed SPID-Chain framework offers a new approach to achieving interoperability within Web3 ecosystems. By structuring a DAG of blockchains, SPID-Chain uses this DAG for inter-consensus processes while incorporating EDSC and Polar codes for intra-consensus operations. This design effectively tackles the scalability, security, and decentralization issues that are common in existing blockchain interoperability solutions. Our extensive simulations confirm that SPID-Chain performs robustly, demonstrating its potential for enabling secure and seamless interactions across multiple blockchains.

REFERENCES

- [1] Liu, Z., Yan, Z., Yang, B., Shen, Y., Zhang, H., and Jia, W. 2022. Make Web3.0 connected. *IEEE Transactions on Dependable and Secure Computing* 19, 5 (Sept.–Oct. 2022), 2965–2981. DOI:<https://doi.org/10.1109/TDSC.2021.3079315>
- [2] Qin, R., Wu, Y., Li, X., Wang, G., Yu, J., Yu, H., and Tian, Y. 2023. Web3-based decentralized autonomous organizations and operations: Architectures, models, and mechanisms. *IEEE Transactions on Systems, Man, and Cybernetics: Systems* 53, 4 (April 2023), 2073–2082. DOI:<https://doi.org/10.1109/TSMC.2022.3228530>
- [3] Liu, Z., Chai, W., Wang, Z., Wu, H., Li, X., Li, X., Liang, K., Xu, Z., He, J., Yang, B., and Jia, W. 2019. HyperService: Interoperability and programmability across heterogeneous blockchains. In *Proceedings of the 2019 ACM SIGSAC Conference on Computer and Communications Security (CCS '19)*. ACM, New York, NY, 549–566. DOI:<https://doi.org/10.1145/3319535.3363136>
- [4] Bernabé-Rodríguez, J., Garreta, A., and Lage, O. 2024. A Decentralized Private Data Marketplace using Blockchain and Secure Multi-Party Computation. *ACM Transactions on Privacy and Security*, 27, 2, Article 19, 29 pages. DOI:<https://doi.org/10.1145/3652162>.
- [5] Mohanty, S. K., and Tripathy, S. 2024. Flexichain: Flexible Payment Channel Network to Defend Against Channel Exhaustion Attack. *ACM Transactions on Privacy and Security*, 27, 4, Article 30, 26 pages. DOI:<https://doi.org/10.1145/3687476>.
- [6] Chen, C., Liu, Z., Zhou, Y., Cai, M., Xu, F., Hu, S., Liu, C., Guo, R., Lian, X., Zhou, H., Yang, Y., and Liu, Z. 2022. When digital economy meets Web3.0: Applications and challenges. *IEEE Open Journal of the Computer Society* 3 (2022), 233–245. DOI:<https://doi.org/10.1109/OJCS.2022.3217565>
- [7] Otoni, R., Marescotti, M., Alt, L., Eugster, P., Hyvärinen, A., and Sharygina, N. 2023. A Solicitous Approach to Smart Contract Verification. *ACM Transactions on Privacy and Security*, 26, 2, Article 15, 28 pages. DOI:<https://doi.org/10.1145/3564699>.
- [8] Cao, L. 2022. Decentralized AI: Edge intelligence and smart blockchain, metaverse, Web3, and DeSci. *IEEE Intelligent Systems* 37, 3 (May/June 2022), 6–19.
- [9] Qiao, Y., Wu, K., and Khabbazian, M. 2024. Non-intrusive Balance Tomography Using Reinforcement Learning in the Lightning Network. *ACM Transactions on Privacy and Security*, 27, 1, Article 12, 32 pages. DOI:<https://doi.org/10.1145/3639366>.
- [10] Chen, Y., and Bellavitis, C. 2020. Blockchain disruption and decentralized finance: The rise of decentralized business models. *Journal of Business Venturing Insights* 13 (2020), e00151. DOI:<https://doi.org/10.1016/j.jbvi.2019.e00151>
- [11] Han, X., Yuan, Y., and Wang, F.-Y. 2019. A blockchain-based framework for central bank digital currency. In *Proceedings of the IEEE International Conference on Service Operations and Logistics, and Informatics (SOLI)*. 263–268. DOI:<https://doi.org/10.1109/SOLI48380.2019.8955032>
- [12] Abeyratne, S. A., and Monfared, R. P. 2016. Blockchain ready manufacturing supply chain using distributed ledger. *International Journal of Research in Engineering and Technology* 5, 9 (2016), 1–10. DOI:<https://doi.org/10.15623/ijret.2016.0509001>
- [13] Agbo, C. C., Mahmoud, Q. H., and Eklund, J. M. 2019. Blockchain technology in healthcare: A systematic review. *Healthcare* 7, 2 (2019), 56. DOI:<https://doi.org/10.3390/healthcare7020056>
- [14] McGhin, T., Choo, K. R., Liu, C. Z., and He, D. 2019. Blockchain in healthcare applications: Research challenges and opportunities. *Journal of Network and Computer Applications* 135 (2019), 62–75. DOI:<https://doi.org/10.1016/j.jnca.2019.02.027>
- [15] Tian, H., Tang, Q., Wang, J., Jia, J., and Wang, S. 2021. Enabling cross-chain transactions: A decentralized cryptocurrency exchange protocol. *IEEE Transactions on Information Forensics and Security* 16 (2021), 3928–3941. DOI:<https://doi.org/10.1109/TIFS.2021.3096124>
- [16] Braun, L., Demmler, D., Schneider, T., and Tkachenko, O. 2022. MOTION – A Framework for Mixed-Protocol Multi-Party Computation. *ACM Transactions on Privacy and Security*, 25, 2, Article 8, 35 pages. DOI:<https://doi.org/10.1145/3490390>.
- [17] Ren, K., Guan, Z., Yang, C., Liu, Y., Zheng, Z., and Yu, J. 2023. Interoperability in blockchain: A survey. *IEEE Transactions on Knowledge and Data Engineering* 35, 12 (Dec. 2023), 12750–12769. DOI:<https://doi.org/10.1109/TKDE.2023.3275220>
- [18] Gazi, P., Kiayias, A., and Zindros, D. 2019. Proof-of-stake sidechains. In *Proceedings of the IEEE Symposium on Security and Privacy*. 139–156. DOI:<https://doi.org/10.1109/SP.2019.00040>
- [19] Lerner, S. D. 2019. RSK: Bitcoin powered smart contracts. [Online]. Available: <https://bit.ly/3OPKof>
- [20] Garoffolo, A., Kaidalov, D., and Oliyynykov, R. 2020. Zendo: A zk-SNARK verifiable cross-chain transfer protocol enabling decoupled and decentralized sidechains. In *Proceedings of the IEEE 40th International Conference on Distributed Computing Systems (ICDCS)*. 1257–1262. DOI:<https://doi.org/10.1109/ICDCS47774.2020.00161>
- [21] Tian, H., Tang, Q., Wang, J., Jia, J., and Wang, S. 2021. Enabling cross-chain transactions: A decentralized cryptocurrency exchange protocol. *IEEE Transactions on Information Forensics and Security* 16 (2021), 3928–3941. DOI:<https://doi.org/10.1109/TIFS.2021.3096124>
- [22] Wang, K., Zhang, Z., and Kim, H. S. 2018. ReviewChain: Smart contract based review system with multi-blockchain gateway. In *Proceedings of the IEEE International Conference on Internet of Things (iThings)*. 1521–1526.

- [23] Xiong, A., Liu, G., Zhu, Q., Jing, A., and Loke, S. W. 2022. A notary group-based cross-chain mechanism. *Digital Communications and Networks* 8 (2022), 1059–1067. DOI:<https://doi.org/10.1016/j.dcan.2022.04.012>
- [24] Ren Project. 2022. RenVM white paper. [Online]. Available: <https://github.com/renproject/ren/wiki>
- [25] Scheid, E. J., Hegnauer, T., Rodrigues, B., and Stiller, B. 2019. Bifrost: A modular blockchain interoperability API. In *Proceedings of the IEEE 44th Conference on Local Computer Networks (LCN)*. 332–339. DOI:<https://doi.org/10.1109/LCN44214.2019.8990860>
- [26] Nolan, T. 2013. Alt chains and atomic transfers. In *Bitcoin Forum*. [Online]. Available: <https://archive.ph/wWzna>
- [27] Herlihy, M. 2018. Atomic cross-chain swaps. In *Proceedings of the ACM Symposium on Principles of Distributed Computing (PODC)*. 245–254. DOI:<https://doi.org/10.1145/3212734.3212736>
- [28] Pillai, B., Biswas, K., Hóu, Z., and Muthukkumarasamy, V. 2021. Burn-to-claim: An asset transfer protocol for blockchain interoperability. *Computer Networks* 200 (2021), 108495. DOI:<https://doi.org/10.1016/j.comnet.2021.108495>
- [29] Ethereum Foundation. 2017. BTCRelay: Ethereum contract for Bitcoin SPV. [Online]. Available: <https://github.com/ethereum/btcrelay>
- [30] Zamyatin, A., Harz, D., Lind, J., Panayiotou, P., Gervais, A., and Knottenbelt, W. J. 2019. XCLAIM: Trustless, interoperable, cryptocurrency-backed assets. In *Proceedings of the IEEE Symposium on Security and Privacy*. 193–210. DOI:<https://doi.org/10.1109/SP.2019.00085>
- [31] Westerkamp, M., and Diez, M. 2022. Verily: A verifiable proof of stake chain relay. *arXiv preprint arXiv:2201.08697*.
- [32] Bentov, I., Ji, Y., Zhang, F., Breidenbach, L., Daian, P., and Juels, A. 2019. Tesseract: Real-time cryptocurrency exchange using trusted hardware. In *Proceedings of the 2019 ACM SIGSAC Conference on Computer and Communications Security (CCS '19)*. ACM, New York, NY, 1521–1538. DOI:<https://doi.org/10.1145/3319535.3363221>
- [33] Interledger Foundation. 2020. Interledger Protocol V4 (ILPv4). [Online]. Available: <https://archive.ph/QZSOR>
- [34] Perun Network. 2022. The Perun framework. [Online]. Available: <https://archive.ph/VpMW1>
- [35] Abebe, E., et al. 2019. Enabling enterprise blockchain interoperability with trusted data transfer (industry track). In *Proceedings of the 20th International Middleware Conference Industrial Track*. 29–35. DOI:<https://doi.org/10.1145/3366626.3368129>
- [36] Pupyshev, A., Dzhafarov, E., Sapranidi, I., Kardanov, I., Khalilov, S., and Laureyssens, S. 2020. Gravity: A blockchain-agnostic cross-chain communication and data oracles protocol. *arXiv preprint arXiv:2007.00966*.
- [37] Pupyshev, A., Dzhafarov, E., Sapranidi, I., Kardanov, I., Khalilov, S., and Laureyssens, S. 2020. SuSy: A blockchain-agnostic cross-chain asset transfer gateway protocol based on Gravity. *arXiv preprint arXiv:2008.13515*.
- [38] Ge, Z., Loghini, D., Ooi, B. C., Ruan, P., and Wang, T. 2022. Hybrid blockchain database systems: Design and performance. *Proceedings of the VLDB Endowment* 15, 5 (2022), 1092–1104. DOI:<https://doi.org/10.14778/3510397.3510406>
- [39] Dinh, T. T. A., Liu, R., Zhang, M., Chen, G., Ooi, B. C., and Wang, J. 2018. Untangling blockchain: A data processing view of blockchain systems. *IEEE Transactions on Knowledge and Data Engineering* 30, 10 (Oct. 2018), 2003–2024. DOI:<https://doi.org/10.1109/TKDE.2018.2831687>
- [40] Amiri, M. J., Agrawal, D., and Abbadi, A. E. 2019. CAPER: A cross-application permissioned blockchain. *Proceedings of the VLDB Endowment* 12, 11 (2019), 1385–1398. DOI:<https://doi.org/10.14778/3342263.3342275>
- [41] Ramakrishna, V. 2021. Meet Weaver, one of the new Hyperledger Labs taking on cross-chain and off-chain operations. [Online]. Available: <https://archive.ph/rYjCg>
- [42] CertiK Security Leaderboard. 2022. Wormhole token bridge attack. [Online]. Available: <https://archive.ph/FAoFG>
- [43] Poly Network. 2022. The analysis and Q and A of Poly Network being hacked. [Online]. Available: <https://archive.ph/NCXGS>
- [44] Conti, M., Kumar, E. S., Lal, C., and Ruj, S. 2018. A survey on security and privacy issues of Bitcoin. *IEEE Communications Surveys and Tutorials* 20, 4 (Fourth Quarter 2018), 3416–3452. DOI:<https://doi.org/10.1109/COMST.2018.2842460>
- [45] Ren, M., et al. 2021. Empirical evaluation of smart contract testing: What is the best choice? In *Proceedings of the 30th ACM SIGSOFT International Symposium on Software Testing and Analysis (ISSTA '21)*. ACM, New York, NY, 566–579. DOI:<https://doi.org/10.1145/3460319.3464837>
- [46] Kaleem, M., Kasichainula, K., Karanjai, R., Xu, L., Gao, Z., Chen, L., and Shi, W. 2021. An event-driven framework for smart contract execution. In *Proceedings of the 15th ACM International Conference on Distributed and Event-based Systems (DEBS '21)*. ACM, New York, NY, 78–89. DOI:<https://doi.org/10.1145/3465480.3466924>
- [47] Müller, S., Penzkofer, A., Polyanskii, N., Theis, J., Sanders, W., and Moog, H. 2022. Tangle 2.0 leaderless Nakamoto consensus on the heaviest DAG. *IEEE Access* 10 (2022), 105807–105842. DOI:<https://doi.org/10.1109/ACCESS.2022.3213121>
- [48] Bartan, B., and Pilanci, M. 2019. Straggler resilient serverless computing based on polar codes. In *Proceedings of the 57th Annual Allerton Conference on Communication, Control, and Computing (Allerton)*.
- [49] Pilanci, M. 2022. Computational polarization: An information-theoretic method for resilient computing. *IEEE Transactions on Information Theory* 68, 4 (April 2022), 2211–2238. DOI:<https://doi.org/10.1109/TIT.2021.3139009>
- [50] Fathollahi, D., and Mondelli, M. 2022. Polar coded computing: The role of the scaling exponent. In *Proceedings of the IEEE International Symposium on Information Theory (ISIT)*. 2154–2159.

- [51] Substrate. The blockchain framework for a multichain future. [Online]. Available: <https://substrate.io/>
- [52] IOTA Foundation. Goshimmer Docker network tools. [Online]. Available: <https://github.com/iotaedger/goshimmer/tree/develop/tools>
- [53] Goshimmer Orphanage. [Online]. Available: <https://github.com/daria305/goshimmer-orphanage>
- [54] Rust Programming Language. [Online]. Available: <https://www.rust-lang.org/>
- [55] Libsodium documentation. [Online]. Available: <https://doc.libsodium.org/>
- [56] Google Cloud. Ethereum BigQuery public dataset for smart contract analytics. [Online]. Available: <https://cloud.google.com/blog/products/data-analytics/ethereum-bigquery-public-dataset-smart-contract-analytics>
- [57] Dziubałtowska, D. 2022. The security of the Coordicide: The implementation and analysis of possible attack vectors. *arXiv preprint arXiv:2205.12568*.
- [58] Lin, Q., Li, C., Zhao, X., and Chen, X. 2021. Measuring decentralization in Bitcoin and Ethereum using multiple metrics and granularities. In *Proceedings of the IEEE 37th International Conference on Data Engineering Workshops (ICDEW)*. 80–87.
- [59] Müller, S., Amigo, I., Reiffers-Masson, A., and Ruano-Rincón, S. 2023. Stability of local tip pool sizes. *arXiv preprint arXiv:2302.01625*.